

Exploring the convective grey zone with regional simulations of a cold air outbreak

Paul R. Field,^{a,k*} Radmila Brožková,^b Ming Chen,^c Jimmy Dudhia,^c Christine Lac,^d Tabito Hara,^e Rachel Honnert,^f Joe Olson,^g Pier Siebesma,^h Stephan de Roode,ⁱ Lorenzo Tomassini,^a Adrian Hill^a and Ron McTaggart-Cowan^j

^aMet Office, Exeter, UK

^bCHMI – NWP, Prague, Czech Republic

^cNational Center for Atmospheric Research, Boulder, CO, USA

^dMétéo-France - CNRM/GMME/MESONH, Toulouse, France

^eNumerical Prediction Division, Japan Meteorological Agency, Tokyo, Japan

^fMétéo-France, Toulouse, France

^gNOAA-ESRL – GSD, Boulder, CO, USA

^hKNMI, De Bilt, Netherlands

ⁱDelft University of Technology, Netherlands

^jNumerical Weather Prediction Research Section, Environment and Climate Change, Canada

^kUniversity of Leeds, ICAS, Leeds, UK

*Correspondence to: P. R. Field, Met Office, FitzRoy Road, Exeter EX1 3PB. E-mail: paul.field@metoffice.gov.uk

This article is published with the permission of the Controller of HMSO and the Queen's Printer for Scotland.

Cold air outbreaks can bring snow to populated areas and can affect aviation safety. Shortcomings in the representation of these phenomena in global and regional models are thought to be associated with large systematic cloud-related radiative flux errors across many models. In this study, nine regional models have been used to simulate a cold air outbreak case at a range of grid spacings (1–16 km) with convection represented explicitly or by a parametrization. Overall, there is more spread between model results for the simulations in which convection is parametrized when compared to simulations in which convection is represented explicitly. The quality of the simulations of both the stratocumulus and the convective regions of the domain are assessed with observational comparisons 24 h into the simulation. The stratocumulus region is not well reproduced by the models, which tend to predict open cell convection with increasing resolution rather than stratocumulus. For the convective region the model spread reduces with increased resolution and there is some improvement in comparison to observations. Comparing models that have the same physical parametrizations or dynamical core suggest that both are important for accurately reproducing this case.

Key Words: grey zone; convection permitting models

Received 25 November 2016; Revised 20 June 2017; Accepted 21 June 2017; Published online in Wiley Online Library

1. Introduction

Many operational centres are now making use of km-scale models to carry out numerical weather prediction (NWP; Maillhot *et al.*, 2010; Brousseau *et al.*, 2016; Clark *et al.*, 2016). The models at these grid resolutions are considered to be convection-permitting and generally do not use a convective parametrization. The difficulty facing these models is that, although they do explicitly convect, they are not at high enough resolution to accurately represent the full spectrum of convective motions (Bryan *et al.*, 2003).

It has long been recognised that a given phenomenon is explicitly resolved for model resolutions much finer than the size, l , of the phenomenon. Likewise, at resolutions much coarser

than l , the phenomenon becomes unresolved and its effect on the resolved large-scale flow can only indirectly be represented through parametrizations. Consequently, around the scale l there exists a range of model resolutions for which the phenomenon is only partly resolved. This range of resolutions is often referred to as the Grey Zone.

Current global NWP models typically do not yet include grey zone convection schemes. The companion intercomparison study with global NWP models suggests that conventional convection parametrizations remove atmospheric instability too easily and prevent models from resolving part of the vertical overturning explicitly even at high resolutions (Tomassini *et al.*, 2017). Another important aspect in the context of the Grey Zone

parametrization problem is the issue of physical parametrization interferences. The global model intercomparison shows that, in the cold-air outbreak case, convection and boundary-layer parametrizations strongly interact, which makes it impossible to restrict the grey zone parametrization problem only to the convection scheme. Indeed, many traditional convection parametrizations even include separate components, like shallow, mid-level, and deep convection schemes, which might reciprocally affect each other. Therefore a unified approach is needed when it comes to addressing scale-adaptivity in the convective Grey Zone. Moreover, the important role of ice-microphysical processes and related precipitation formation hamper an unambiguous assessment of the impact of model resolution on the simulated cloud and boundary-layer structures in the cold air outbreak case.

At resolutions finer than 10 km, the scale depth of the atmosphere, convective overturning starts to become resolved. Convection is a truly multiscale phenomenon ranging from the deep convective towers of 10 km to the smallest turbulent eddies of a few mm at the Kolmogorov scale. Therefore, the Grey Zone of convection encompasses a wide range of scales, so that refining the resolution in the Grey Zone leads to a continuous enrichment of the resolved convective processes. The fundamental question is how to parametrize the unresolved part of the convection in the Grey Zone in such a way that a parametrization is aware of the resolution and the part of the convection that is resolved.

For resolutions finer than a few hundred metres this is realized through an eddy diffusivity approach where the model resolution is used as a length-scale in the eddy diffusivity coefficient. This classic Smagorinsky closure describes how the effect of the parametrized turbulent diffusion decreases with increasing resolution and is based on the self-similar energy cascade of three-dimensional turbulence in the inertial subrange of the convective boundary layer.

However, resolutions in the range between 500 m and 5 km are outside the inertial subrange and consequently the classic Smagorinsky closure is not applicable anymore. The moist convective processes that operate at these resolutions are usually parametrized through convection parametrizations that in general do not have a scale-aware formulation. Instead it is common practice for models operating in the convective Grey Zone to simply switch off the convection parametrization somewhere in the resolution range between 500 m and 5 km.

Previous exploration of the Grey Zone has focused on deeper convection in the Tropics. The CASCADE project included simulations at resolution of 40, 12, 4, 1.5 km over West Africa and the tropical Pacific. Generally it was found for the West African land-based simulations that coarse resolution (12 km) with convection parametrization switched off produced a better timed diurnal behaviour and subsequently agreed better with satellite-based radar (Stein *et al.*, 2015) and radiative flux measurements (Pearson *et al.*, 2014). These studies over land and another over the tropical Pacific (Holloway *et al.*, 2012) concluded that the highest resolution simulations with convection explicitly resolved agreed best with observations. Similarly, Gao *et al.* (2017) report improved representation of precipitation spatial distribution and timing in higher resolution (4 km when compared to 12 and 36 km). These results suggest that, at least for deep convection, we should expect better comparison to observations at higher resolution. For shallow convection the convective flows that develop in km-scale models are grid-scale-dependent and under-resolved (Sakradzija *et al.*, 2016), necessitating the implementation of stochastic treatment that modifies the resolved flows and aims to better represent higher-order moments of the motions.

In order to accelerate research of model simulations of moist convection in the Grey Zone, the Working Group on Numerical Experimentation (WGNE) in collaboration with the Global Energy and Water cycle Exchanges (GEWEX) Global Atmospheric Systems Study (GASS) panel has initiated a Grey Zone project that aims to analyse and improve convection parametrizations

that operate at resolutions in the Grey Zone. A cold air outbreak situation has been selected as a first case to explore the behaviour of the convective parametrizations in the Grey Zone.

Correctly simulating cold air outbreaks is important for weather forecasting. From a regional perspective they tend to be multi-day events that can bring snow to populated areas. Moreover, they are known to be associated with lightning that affects aviation safety (Wilkinson *et al.*, 2013) and icing conditions that create hazards for marine vessels (Moore, 2013). They are a challenge to km-scale models because the boundary layer is shallow, but the horizontal open- and closed-cell mesoscale structures associated with the cold air outbreak can reach scales up to almost 100 km. The question is whether these observed mesoscale structures can be realistically reproduced by km-scale models. Shortcomings in the representation of cold air outbreaks in climate models have been identified as leading to systematic errors in liquid water and broadband fluxes (Bodas-Salcedo *et al.*, 2014). These errors have implications for sea ice and the general circulation (Hwang and Frierson, 2013).

The cold air outbreak weather situation is unique in that it mixes the difficulties inherent in resolving boundary layer, convective structures, microphysics and their interactions. This study uses a novel application of a wide range of different model resolutions in tandem with structural model changes controlled by switching convective parametrizations on or off to explore the ability of NWP models to provide robust forecasts across the edge of the convective Grey Zone. In this paper the following questions are asked:

- (i) How well do km-scale regional models resolve and simulate the evolution of a cold air outbreak?
- (ii) What is the effect of grid resolution on the ability of the model to represent a cold air outbreak?
- (iii) Are model physics or dynamical formulations more important for the fidelity of the simulation?
- (iv) Are convective parametrizations required for km-scale simulations?

2. Description of the case

The case is from 31 January 2010 and has been described in Field *et al.* (2014). It is a cold air outbreak located between Iceland, Norway and Scotland. It is characterized by a polar low feature at 64°N, 4°W to the west of Norway, and a high pressure ridge stretching between the Azores and Iceland (Figure 1(a)). There is a strong northerly flow between Iceland and Norway, stretching from north of 70°N to south of 60°N over the UK. This synoptic situation follows the climatological pattern identified for cold air outbreaks in the Greenland–Iceland–Norwegian sea areas by Kolstad *et al.* (2009).

The flow brings cold air from the Arctic sea ice over the warmer (5–10°C) seas to the south. Parcels traverse ~700 km in 12 h (~15 m s⁻¹). Northwest of the Faroe Islands the boundary layer is ~1 km deep and characterized by a stratocumulus cloud deck with close to complete cloud cover. Droplet concentrations from satellite-based estimates are 50–100 cm⁻³. Even though the stratocumulus region is over colder sea than the convective region, there is likely to be little ice, but there were no *in situ* observations to confirm this. The reason for this dearth of ice in the stratocumulus region relative to the convective region is potentially linked to the higher cloud-top temperatures and hence reduced heterogeneous nucleation rates than for the deeper colder-topped convective cloud. Liquid water paths reached ~0.3 kg m⁻² based on remote-sensing estimates. Eventually, as the air moves over warmer sea, the boundary layer begins to grow and the stratocumulus cloud gives way to cumulus that reaches up to ~3 km (red box in Figure 1(b)). Aircraft measurements indicate that in the cumulus region the ice concentrations (maximum size, D > 100 μm) reach ~10 L⁻¹ and droplet concentrations ~10 cm⁻³ with ice and liquid water contents of ~0.3 and ~0.1 g m⁻³, respectively. Aircraft-based estimates of integrated water paths

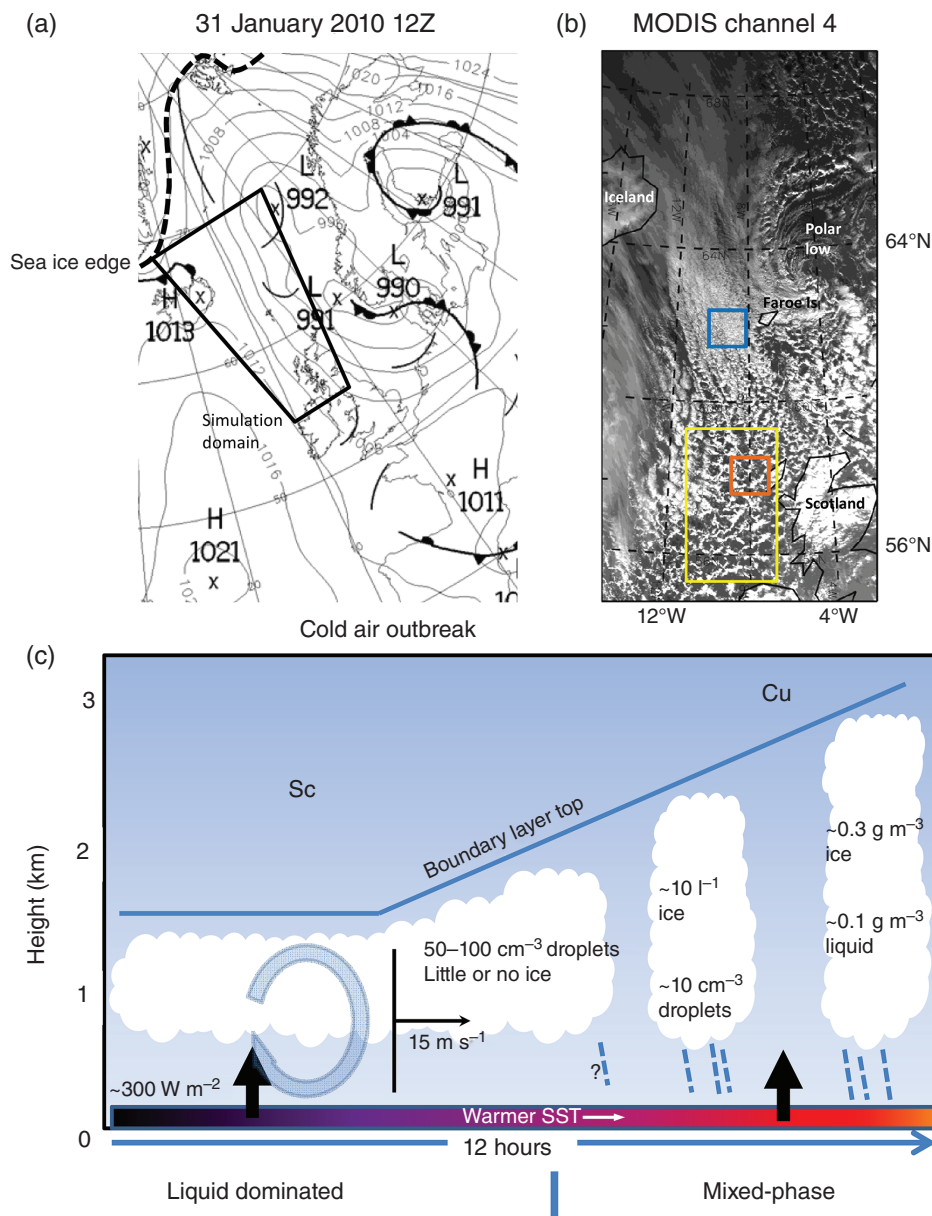


Figure 1. (a) Met Office analysis chart and (b) MODIS image (channel 4, 550 nm) for 1200 UTC 31 January 2010. The blue square indicates the stratocumulus region and the orange box indicates the convective region. The larger yellow box indicates the region used for the rainrate plot in Figure 16. (c) Schematic of the cloud evolution as the air sweeps down over the course of ~ 12 h from the north (left) to the south (right), indicating cloud morphology and gross properties including hydrometeor concentrations, wind speed, boundary-layer height and total sensible plus latent heat flux. Sea ice extent from <http://igloo.atmos.uiuc.edu>.

for the cumulus region are $0.06 \pm 0.03 \text{ kg m}^{-2}$ for liquid and in the range of $0.08\text{--}0.20 \text{ kg m}^{-2}$ for ice. A schematic of the evolution of the boundary layer and cloud is shown in Figure 1(c).

3. Models

Output from nine different models was submitted for the comparison:

- UM = Unified Model (UK);
- WRF = Weather Research and Forecasting model (USA, two configurations: NCAR and NOAA);
- NHM = non-hydrostatic model (Japan);
- ASUCA = A System based on a Unified Concept for Atmosphere (Japan);
- Meso-NH = mesoscale non-hydrostatic (France);
- AROME = Applications of Research to Operations at Mesoscale (France);
- ALADIN = Aire Limitée Adaptation dynamique Développement International (Czech Republic);
- EC = Environment Canada.

Table 1 summarizes the models and the choices for microphysics, boundary layer, convection and advection. The

models were run with grid spacings of 16, 8, 4, 2, 1 km grid spacing (AROME only 4,2,1) over a domain 1600 km (north–south) \times 800 km (east–west). Sets of simulations were carried out with convection parametrization on (convection-on) and with convection parametrization off (convection-off).

Apart from AROME and ALADIN which used ARPEGE analyses, the models were run for 24 h from the ECMWF analysis (1200 UTC 30 January 2010), with the bulk of the analysis carried out at around 1200 UTC 31 January. Some models used a parent global model to provide boundary conditions to drive the inner nested model used to provide the data for the intercomparison. Other models used 6-hourly ECMWF analyses to provide boundary conditions for a large area regional model which in turn provided boundary conditions for the inner nest used in the intercomparison.

Tests were carried out with the UM to assess the impact of using a different starting analysis and vertical level set. For the sensitivities, a UM analysis was used instead of the ECMWF analysis and for the vertical level sensitivity test the level spacings were halved to increase the number of levels from 70 to 140. The results indicate that, while the changes are systematic, they are the same size as the variability represented in the control run.

Table 1. Description of models used.

A	UM ; Met Office; Walters <i>et al.</i> (2017) GA6(global)OS37(regional); 16/29/70/40 km
B	Wilson and Ballard (1999)
C	Non-local boundary-layer scheme (Lock <i>et al.</i> , 2000)
D	No convection
E	Global model settings for deep shallow and mid convection (Walters <i>et al.</i> , 2017)
F	Semi-Lagrangian (Wood <i>et al.</i> , 2014)
G	Uses the 'Smith cloud scheme' (Smith 1990) to represent subgrid distribution of humidity. It assumes a triangular distribution of humidity with a predefined width (called RHcrit). When the grid box total water mixing ratio/saturated mixing ratio reaches RHcrit (~0.8), cloud can start to form. With increasing water, the cloud fraction in the grid box increases, eventually reaching 1.0.
A	WRF ; NCAR; (Skamarock <i>et al.</i> 2008) 7/14/75/29 km
B	Thompson <i>et al.</i> (2008)
C	YSU PBL
D	–
E	Tiedtke cumulus option
F	ARW dynamical core. Non-hydrostatic, compressible, time-splitting with semi-implicit sound waves, third-order Runge–Kutta (RK) time steps, C-grid staggering, fifth-order horizontal and third-order vertical advection, terrain-following mass-based vertical coordinate.
G	–
A	WRF ; NOAA; Skamarock <i>et al.</i> (2008), Benjamin <i>et al.</i> (2016); 17/25/62/27 km
B	Thompson DM including graupel and hail
C	Mellor–Yamada–Nakanishi–Niino (MYNN) scheme, with modifications to use a non-local BouLac scheme in the free atmosphere and a surface-layer length-scale which varies with surface stability parameter.
D	–
E	Grell–Freitas scheme. Scale-aware scheme, transforms into a shallow-Cu scheme at high resolution (<5 km), and is shut off entirely at grid spacings below 1 km. This is run at every time-step.
F	Same as NCAR, but fifth-order vertical advection instead of third-order.
G	–
A	NHM ; JMA; Saito <i>et al.</i> (2006, 2007); 11/21/58/20 km
B	Physics implemented through 'Physics Library' (Hara <i>et al.</i> , 2012). Six-class single-moment cloud microphysics based on Lin <i>et al.</i> (1983).
C	Improved MYNN scheme (Nakanishi and Niino, 2009)
D	–
E	Kain and Fritsch (1990) (KF) scheme
F	Finite-difference method employing the leap-frog time integration method, fourth-order difference method with an artificial advection correction scheme and linear and nonlinear numerical diffusions.
G	–
A	ASUCA ; JMA; Ishida <i>et al.</i> (2009, 2010); 11/21/58/20 km
B	Physics implemented through 'Physics Library' (Hara <i>et al.</i> , 2012). Six-class single-moment cloud microphysics based on Lin <i>et al.</i> (1983).
C	Improved MYNN scheme (Nakanishi and Niino, 2009)
D	–
E	KF scheme. Uses different triggering at 2 and 1 km resolution
F	Finite-volume method with the third-order RK time integration and upwind third-order advection scheme with a flux limiter and without numerical diffusions.
G	All fields are the sum of the resolved and subgrid. Method 1 forcing driven by dx =20 km global
A	Meso-NH ; CNRM/Météo-France; Lafore <i>et al.</i> (1998); 14/24/45/19 km
B	Mixed-phase one-moment microphysical scheme (Pinty and Jabouille, 1998) with two liquid and three ice categories
C	A prognostic turbulent kinetic energy scheme (1.5 order; Cuxart <i>et al.</i> , 2000) in 1D mode with the Bougeault and Lacarrère (1989) mixing length
D	No deep or shallow convection
E	Deep: the mass flux scheme of Bechtold <i>et al.</i> (2001) at 16, 8 and 4 km. Shallow: an EDMF scheme (Pergaud <i>et al.</i> , 2009) at all resolutions.
F	Eulerian with the fifth-order WENO advection scheme for wind, associated to a third-order RK temporal scheme, and the PPM (Colella and Woodward, 1984) advection scheme for other variables.
G	Method 2, using ECMWF analyses every 6 h to generate LBCs, 45 vertical levels
A	AROME ; CNRM/Météo-France; Seity <i>et al.</i> (2011); 15/26/60/51 km
B	As Meso-NH
C	As Meso-NH
D	No deep or shallow convection
E	Only shallow convection from an EDMF scheme (Pergaud <i>et al.</i> , 2009) at 4, 2 and 1 km
F	Spectral, semi-implicit semi-Lagrangian
G	ARPEGE initial and boundary conditions
A	Aladin ; CHMI; Termonia <i>et al.</i> (2017); 15/27/60/50 km
B	ALARO-0 version. Clouds: a scheme based on the Xu and Randall (1996) approach. Microphysics: a one-moment Kessler type, not published as a whole, but there is an original treatment of the sedimentation problem (Geleyn <i>et al.</i> , 2008).
C	Pseudo-prognostic TKE scheme (Geleyn <i>et al.</i> , 2006). Horizontal diffusion: semi-Lagrangian-based grid-point local diffusion (Vaña <i>et al.</i> , 2008)
D	–
E	Moist deep convection: the 3MT (Modular Multi-scale Microphysics and Transport) scheme, specifically developed for the grey zone of convection (Gerard <i>et al.</i> , 2009). This scheme was switched on or off as the only difference between the two sets of experiments. It is important to note that we use the same microphysics in both cases (3MT on or off); in the case the 3MT is active, we treat both the resolved and sub-grid condensations.
F	Spectral in horizontal, finite differences in vertical. Time scheme and advection: two-time-level semi-implicit semi-Lagrangian (Bénard <i>et al.</i> , 2010)
G	Flux-conservative thermodynamic equations in a mass-weighted framework
A	EC ; Environment Canada; Girard <i>et al.</i> (2014); 5/13/26/29 km
B	Two-moment bulk microphysics (Milbrandt and Yau, 2005a, 2005b) with two liquid categories and four ice categories
C	Prognostic TKE scheme (1.5 order; Bélair <i>et al.</i> , 1999)
D	No deep or shallow convection, but PBL clouds are still active
E	KF scheme for deep convection and a Kuo-type closure for shallow convection (Bélair <i>et al.</i> , 2005). Trigger for deep convection adjusted for the operational system with 2.5 km grid spacing.
F	Gridpoint-based two-time-level implicit semi-Lagrangian.
G	–

A= model; contributor; main reference; levels(1 km/3 km/total/top(km)). B= Microphysics.

C= Boundary layer. D= Convection off. E= Convection on. F= Advection. G= Other remarks.

Four of the models use semi-Lagrangian advection (AROME, ALADIN, EC, UM). For convection, two models use 'global settings' that are almost unchanged for all of the convection-on simulations (WRF-NCAR, UM). Four models have some scale-aware convection treatment (WRF-NOAA, Meso-NH, NHM and ASUCA) either through an approach that gradually shuts off convection as resolution increases (WRF-NOAA), or by not doing deep convection for the higher-resolution simulations (Meso-NH), or by using different convective triggering thresholds at the highest resolutions (NHM, ASUCA).

Interestingly, there are a few pairs of models that either share the same physics or dynamical cores. AROME and Meso-NH have the same physics but different dynamical cores and use different initializations (ARPEGE, ECMWF). Similarly, NHM and ASUCA also have the same physics but different dynamical cores. While two pairs of models (NOAA and NCAR; AROME and ALADIN) share a dynamical core but different microphysics, boundary layer and convection parametrizations.

4. Results

4.1. General comparison

Outgoing long-wave flux at the top of the atmosphere from each model for the 1, 16 km and convection-on and convection-off simulations are shown for T+24 h into the simulation (Figures 2–4). The darker shades represent greater fluxes from warmer surfaces such as the sea surface or clouds lower down in the troposphere. These figures can be compared qualitatively with the image shown in Figure 1(b). Comparison of the 1 km convection-off panels shows that the polar low feature is consistently reproduced in size and location by all of the models. In the southern half of the domain, all of the models show convective clouds. To the northwest of the domain most models show the encroaching cirrus from an extratropical cyclone to the west of the study region. In the northern portion of the domain the models show different low cloud morphologies ranging from cloud streets to more closely packed convection. The 16 km simulations with convection-off again show the polar low to be of similar size and location between models, but there is generally more widespread low cloud. For the convection-on simulations at different resolutions, the results are more varied. This is due in part to different models having varying levels of model resolution awareness built into their convection parametrizations. For the 1 km convection-on results, some models essentially switch off parametrized convection and look the same as the convection-off simulation (ASUCA, AROME, ALADIN, EC, NOAA), while others experience a strong impact from the parametrized convection (Meso-NH, UM, NCAR, NHM).

For more a quantitative comparison, two regions have been focused on: a stratocumulus region in the north (blue box in Figure 1(b)) and a convective region in the south (red box in Figure 1(b)). For each model, mean values and variances are calculated in 100 km regions for the different resolutions and for the case where convection is on or off. These results are then compared with aircraft and satellite observations – Liquid Water Path from the Advanced Microwave Scanning Radiometer (Wentz and Spencer, 1998), and broadband fluxes from the Clouds and the Earth's Radiant Energy System (Wielicki *et al.*, 1996; Field *et al.*, 2014) around 1200 UTC on 31 January 2010.

4.2. Stratocumulus

In this region the satellite observations in Figure 1(b) indicate widespread closed cell layer cloud with almost complete cloud cover. It is clear that most of the 1 km models are not able to reproduce this behaviour and instead tend towards open cellular shallow convection.

Mean outgoing broadband fluxes over a 100 km × 100 km region in the stratocumulus dominated part of the domain for

convection-off simulations are shown in Figure 5 for short- and long-wave. For each model the results for the different model resolutions are given. Results from the convection-off simulations differ from the satellite-observed value and show that the simulated fluxes for both long- and short-wave deviate more from the observations with increasing resolution. There is more model-to-model variability at 1 km than there is at 16 km for the short-wave fluxes. With the convection-on (Figure 6) some models show monotonic changes with increasing resolution, but there is generally less variation across the models and with changing resolution than with the convection-off simulations. For some models (ALADIN, NCAR, Meso-NH) the convection-on simulations agree better with the observations at 1 km than the convection-off simulations, suggesting that the parametrization at these resolutions may still be beneficial. Overall, the simulations have 10–30 W m⁻² (5–15%) too much outgoing long-wave flux and underestimate the outgoing short-wave flux by 20–100 W m⁻² (10–60%), suggesting insufficient cloud cover.

Liquid water path for the convection-off simulations (Figure 7) shows a very wide range that tends to decrease with increasing resolution but also drifts from the observed value. Only two simulations (EC, NOAA) have a value consistent (>0.1 kg m⁻²) with the observations for some resolutions. For convection-on, the liquid water path is lower than for convection-off (Figure 8) and both are generally much lower than the estimate derived from passive microwave observations (Field *et al.*, 2014). There are no observational estimates of ice water path (IWP) for the stratocumulus region. Nevertheless, it can be seen (Figure 7(b)) that the models estimates span an order of magnitude from 0.01 to 0.1 kg m⁻², with no obvious trend with resolution.

Profiles of potential temperature and total water (Figure 9) show that there is less model spread in the 1 km simulations than in the 16 km simulations. For an individual model, the difference between convection on and off is less than the spread between models. Generally, the boundary layer is deeper, warmer and drier for the convection-on simulations relative to the convection-off simulations. This is consistent with parametrized convection more efficiently mixing the boundary layer than when it is done by explicit convection. The profiles look well-mixed in the bottom kilometre of the profile. The top of the boundary layer varies between models over a few hundred metres.

Field *et al.* (2014) demonstrated that modifying the boundary-layer scheme to promote a mixed-layer character in the dynamical conditions experienced in the stratocumulus region leads to improved cloud cover and radiative fluxes. Those changes were not introduced to the operational UM due to the proximity of the northern boundary to the British Isles and have not been included in these results which make use of an operational configuration.

4.3. Cumulus

Concentrating on a convective region to the south, both the convection-off (Figure 10) and convection-on (Figure 11) simulations show a convergence towards the observed long- and short-wave flux values with increased resolution, but with a broader range of simulated long-wave broadband fluxes with convection-on (Figure 11). Generally, for the convective region there is better agreement between the models and the observations of broadband flux than was seen for the stratocumulus region.

For the convection-off simulations, the LWP tends to decrease with increased resolution for most of the models (Figure 12). About a third of the models have LWP values within the range of the observations at the highest model resolution. The rest of the models have lower values (factor of 2–5). The range of LWP spans an order of magnitude and this range across the models is larger than the change seen by each model as a function of resolution. Some of the models which present an underestimation of LWP are in better agreement with the aircraft measurements of IWP,

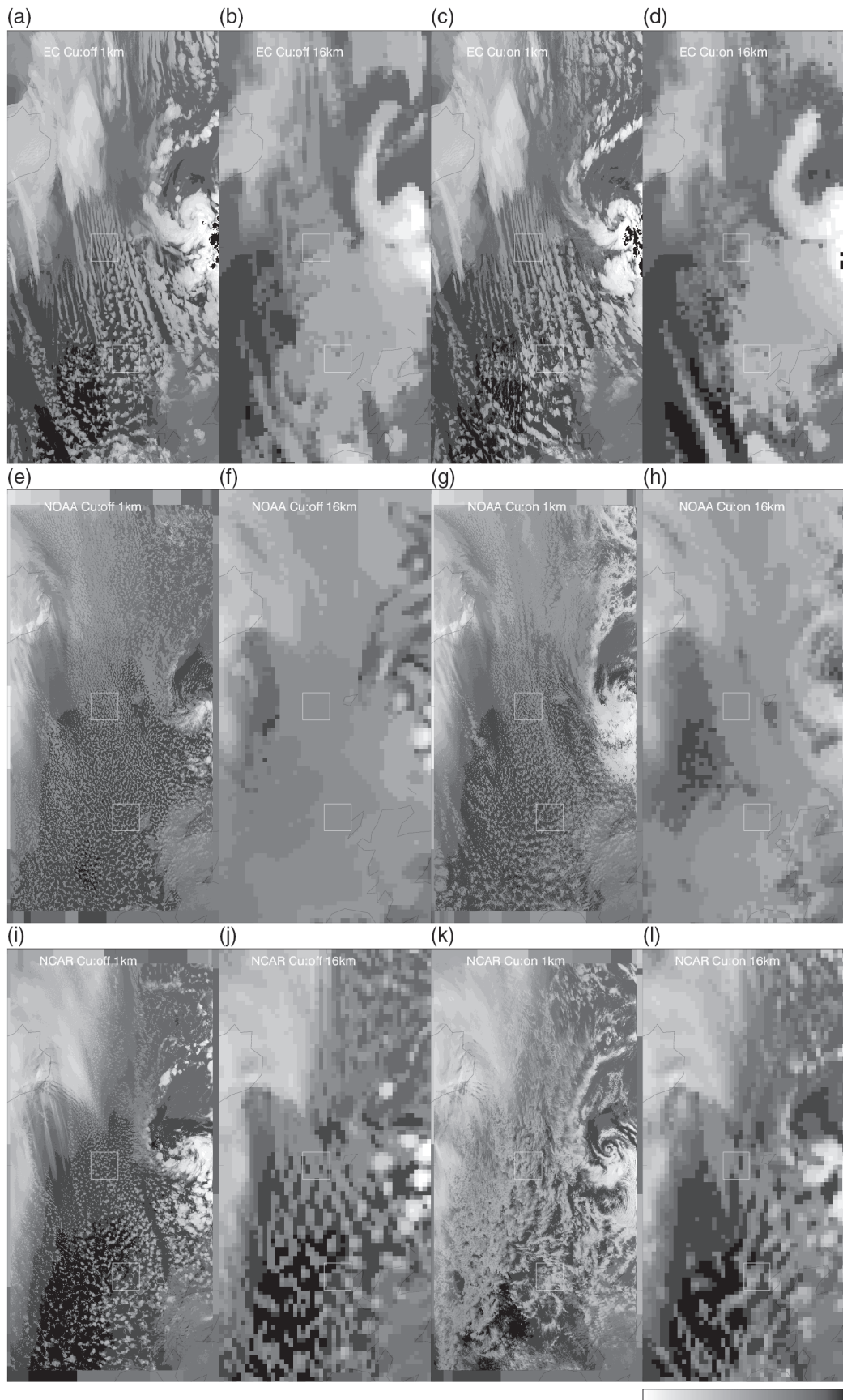


Figure 2. Top of atmosphere outgoing long-wave fluxes from models (a)–(d) EC, (e)–(h) NOAA, (i)–(l) NCAR from a 24 h forecast valid for 1200 UTC 31 January 2010. Each row shows, from left to right, 1 km convection off, 1 km convection on, 16 km convection off, 16 km convection on (except AROME which is 4 km instead of 16 km for lowest resolution).

and only one (ASUCA) presents correct values for both fields. At 1 km resolution, the intermodel spread is high for IWP. Three of the simulations (NCAR, Meso-NH and ASUCA) produce good agreement with the observations (based on integrating the aircraft measurements) and a slight monotonic decrease in IWP with increasing resolution, while the other models exhibit lower

IWP. For convection-on (Figure 13), the results are more variable, but the LWP values are consistently low with only one model (ASUCA) producing similar values to the observations at the 1 km resolution, while two other models (EC and NOAA) have better agreement at the coarsest resolution. The intermodel spread for IWP is reduced with convection-on at 1 km.

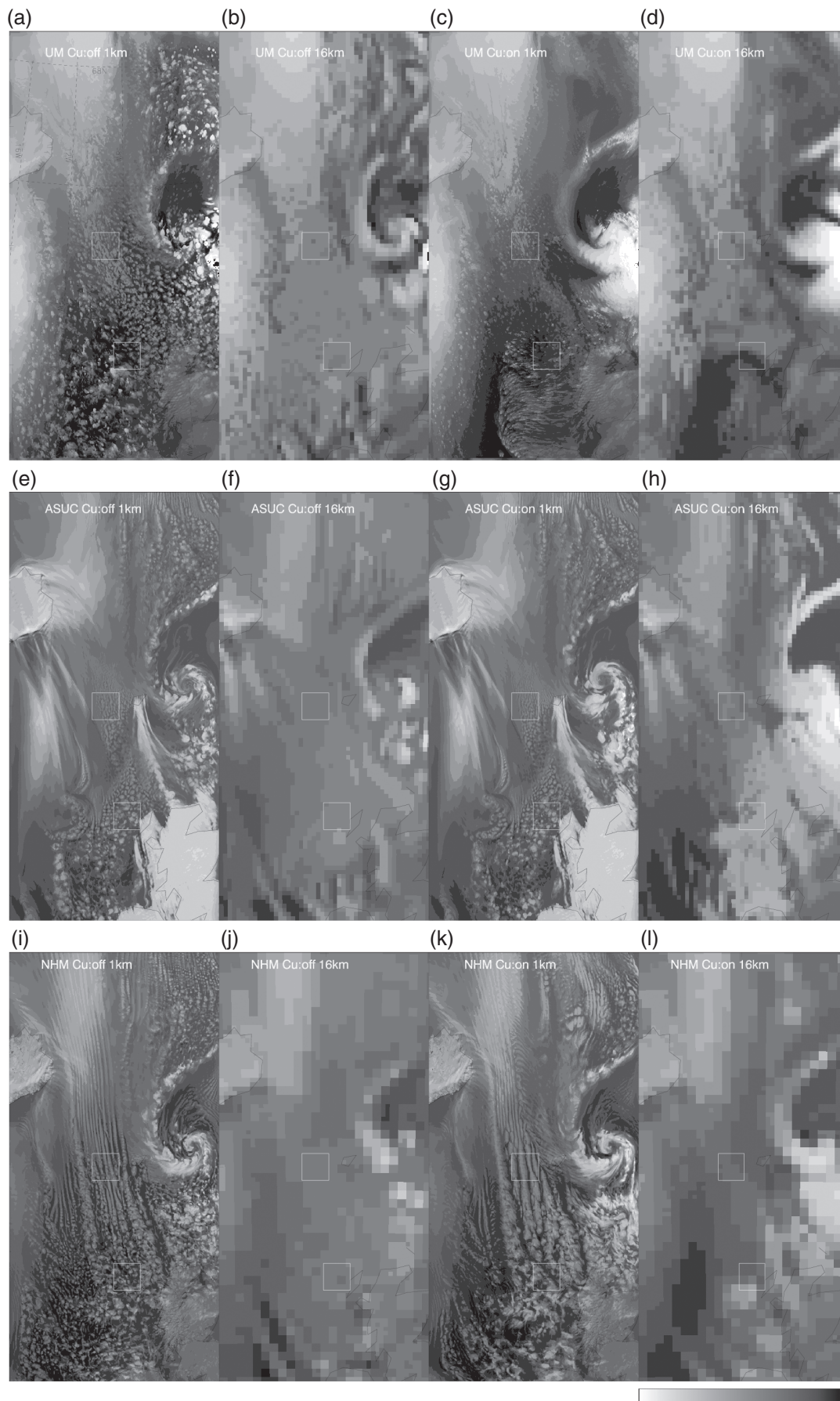


Figure 3. As Figure 2, but for (a)–(d) UM, (e)–(h) ASUCA and (i)–(l) NHM.

Profiles of potential temperature and total water (Figure 14) indicate reduced model spread for the 1 km simulations when compared to the 16 km simulations. The simulations generally agree with the aircraft observations, although the potential temperature in the lowest kilometre tends to be lower for most

of the models than suggested by the observations. For a given model, the difference between convection-on and convection-off simulations is less than inter-model differences. Liquid and ice water content profiles (Figure 15) for the 1 km simulation (16 km simulations exhibit more spread) show a peak in liquid water

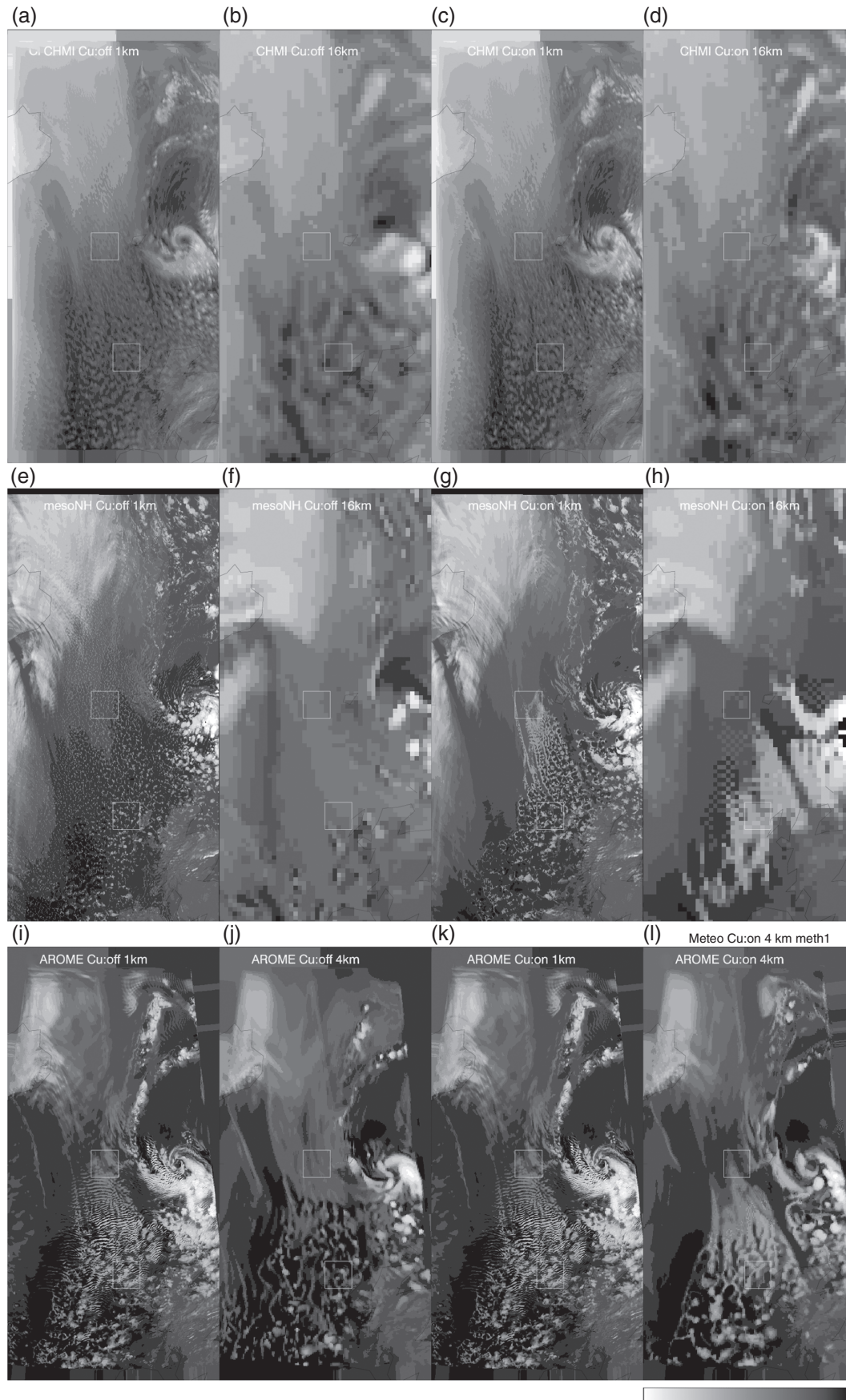


Figure 4. As Figure 2, but for (a)–(d) Aladin, (e)–(h) Meso-NH, and (i)–(l) AROME.

at heights ranging from 1 to 2.5 km. The aircraft observations suggest that the liquid water contents are greatest between 2 and 2.5 km. Some models produce liquid water contents of the same magnitude (0.03 g kg^{-1}) as the aircraft observations, but most do not. The modelled ice water contents are generally smaller than the peak observed ice water contents (0.15 g kg^{-1}). Some of

the convection-on models (Meso-NH, AROME) produce deeper ice water profiles that are closer to the observations than any of the convection-off simulations at 1 km. For the liquid profiles, convection-on generally produces less liquid.

Taking a larger region (yellow box in Figure 1(b)), three snapshots of 10 min rain accumulations at 1100, 1200, 1300 UTC

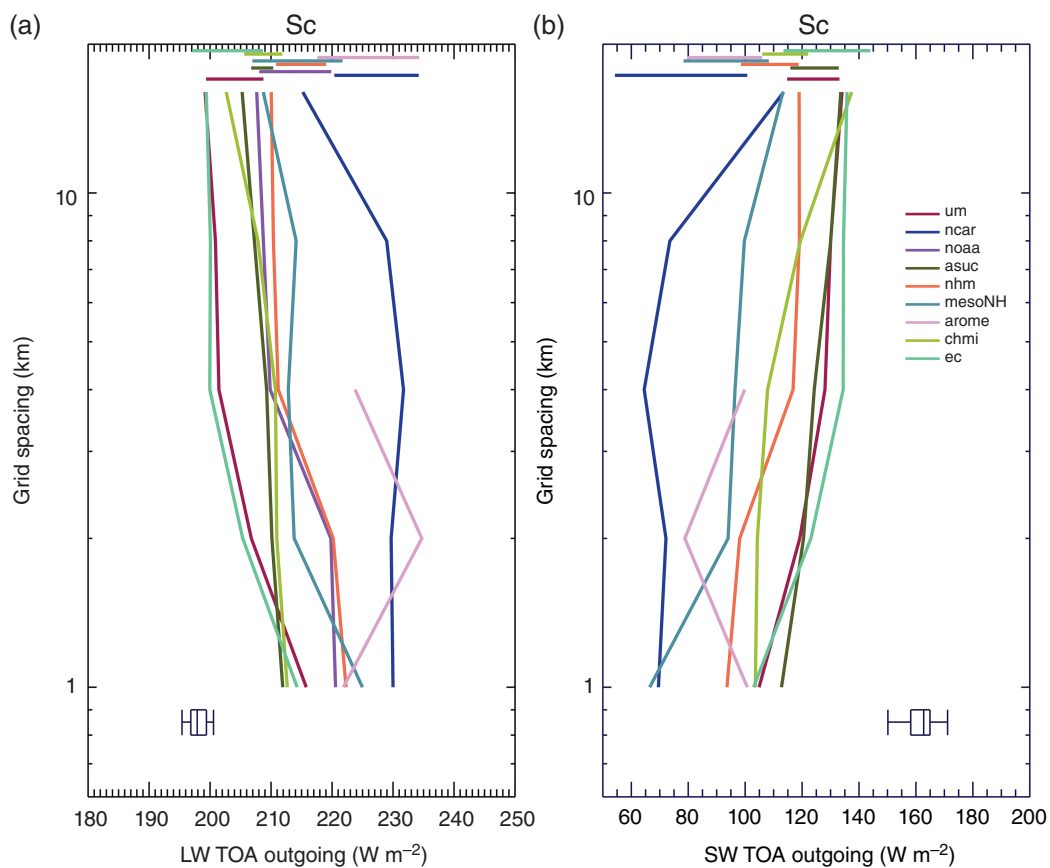


Figure 5. Area-mean values in the 100 km × 100 km stratocumulus region from the convection-off simulations as a function of resolution for (a) long-wave outgoing top of atmosphere (TOA) flux, (b) short-wave outgoing TOA flux. The satellite-derived estimates are given as a whisker plot (5, 25, mean, 75, 95 percentiles). The horizontal bars at the top of the panels indicate the average, across the resolutions, of 2 standard deviations derived from the 100 km box.

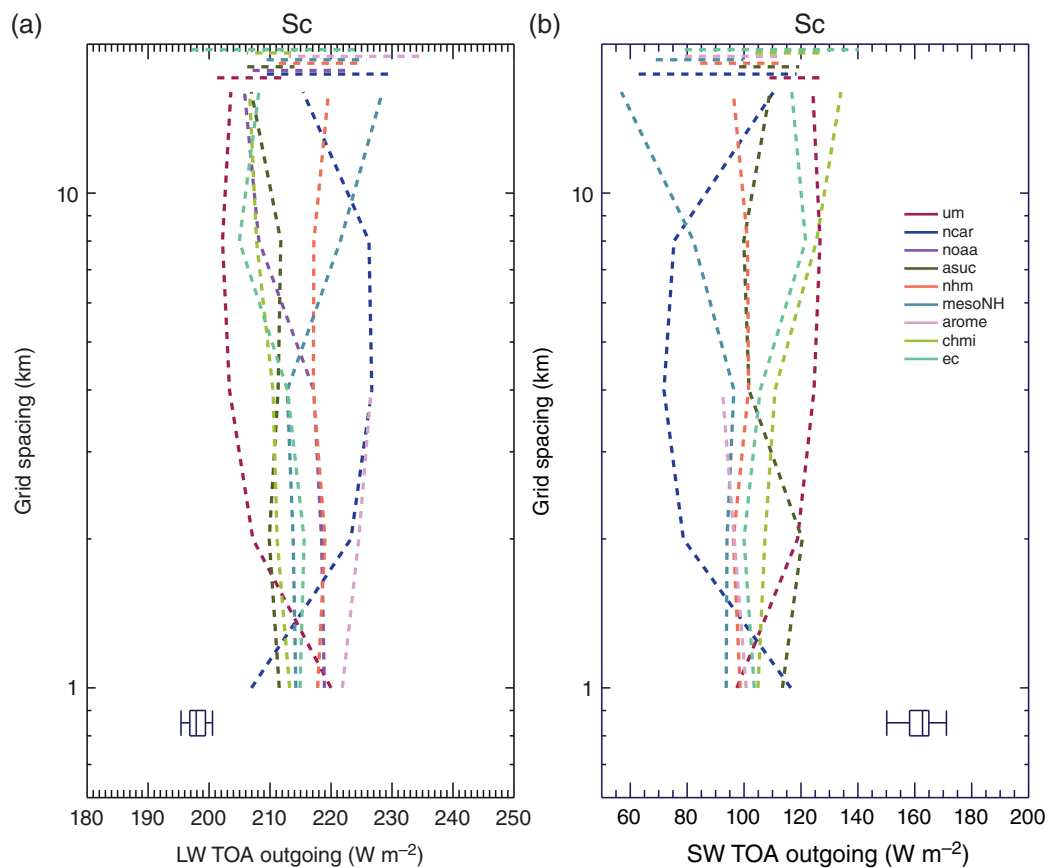


Figure 6. As Figure 5, but with convection ON.

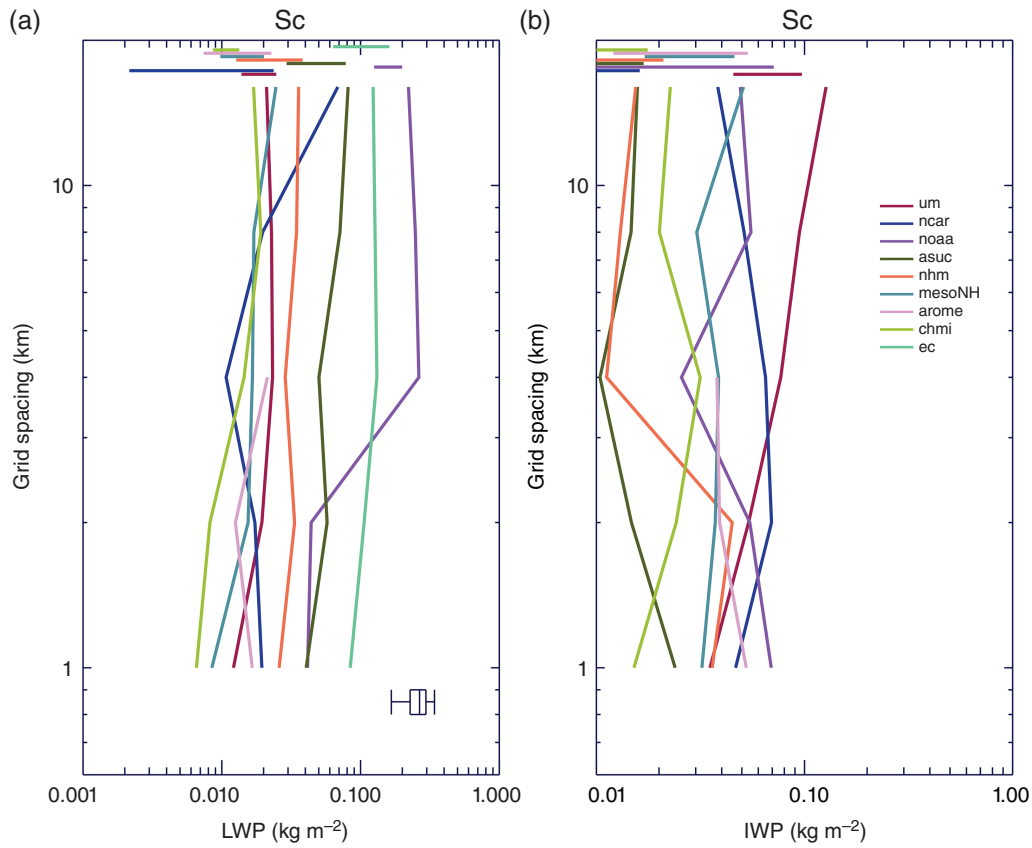


Figure 7. As Figure 5, but for (a) liquid water path, and (b) ice water path.

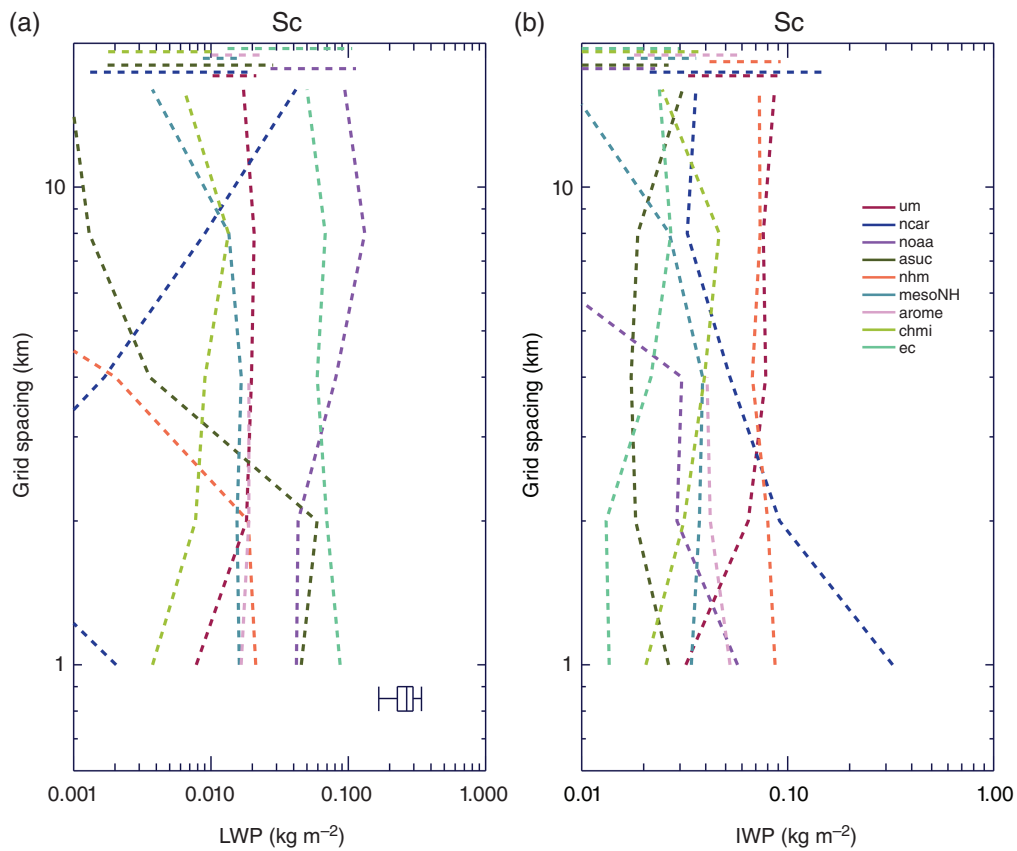


Figure 8. As Figure 7, but with convection ON.

were combined to provide precipitation statistics from each of the models (Figure 16) around the same time as the comparison with observations has been made. Domain-averaged 10 min rain accumulations across all resolutions for all models with convection-off lies within ± 0.09 mm of the multimodel mean of ~ 0.09 mm, and for 1 km, the models lie within ± 0.07 mm of 0.09 mm.

Three models exhibit approximately constant accumulations of rain with changing resolution (ALADIN, NCAR, UM). Most models show a generally increasing monotonic change with increasing resolution, but two models exhibit a distinct peak in rain accumulation at 4 km resolution (NHM, AROME). Results from an earlier version of the UM exhibited a peak in rainrate

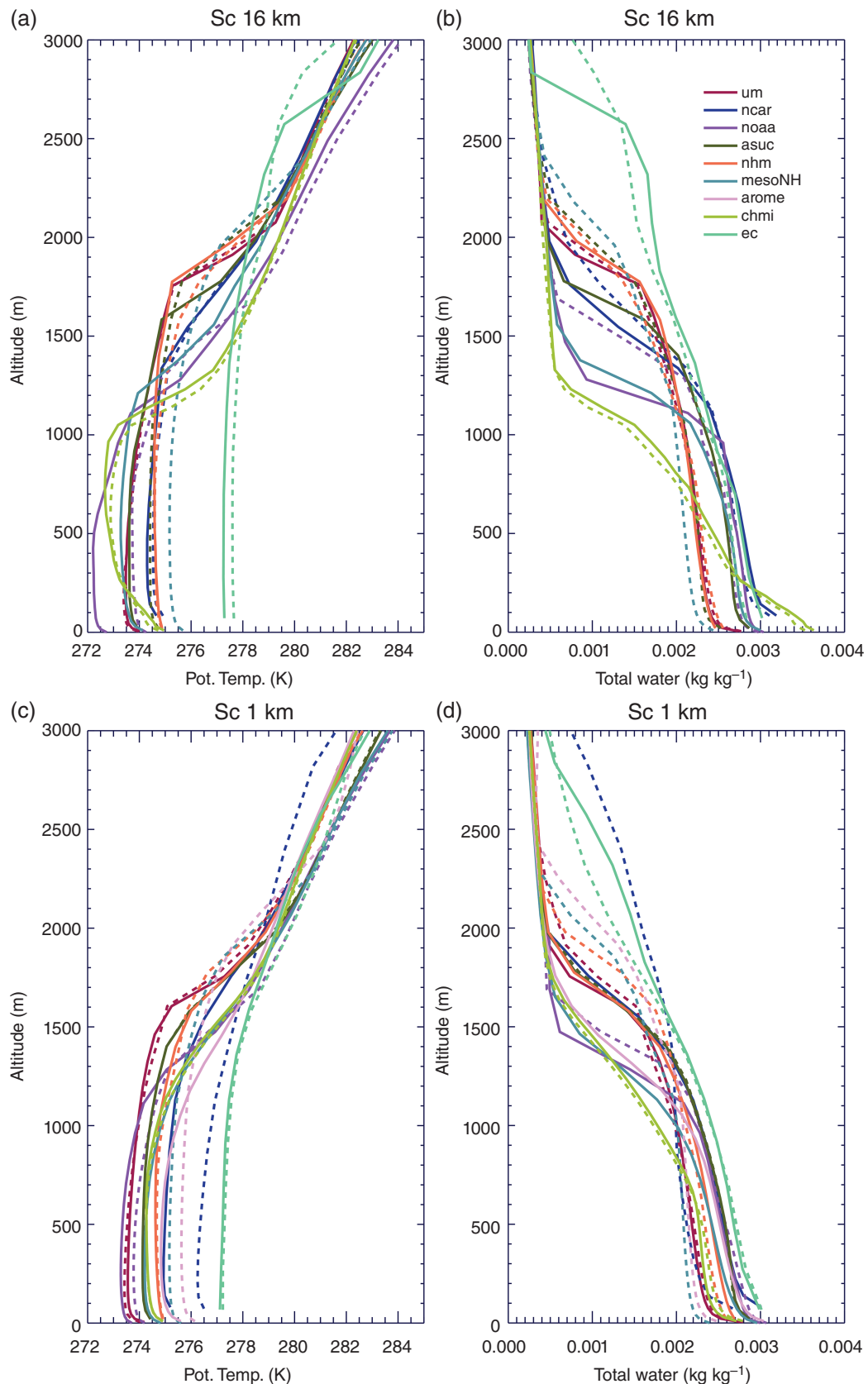


Figure 9. Mean profiles for the stratocumulus region of (a, c) potential temperature and (b, d) total water for (a, b) 16 km resolution simulations and (c, d) 1 km simulations. Solid denotes convection off, and dashed is convection on.

at intermediate resolutions, but the results presented here used enforced moisture conservation for semi-Lagrangian advection (Aranami *et al.*, 2015) which has reduced this tendency. The results from the convection-off simulations exhibit similar values to the convection-on counterpart, but generally present less or little variation with resolution.

Rain accumulations can be explored further by examining histograms. All of the rainrate histograms follow the usual gamma

distribution with lower frequency at larger accumulations. As may have been expected, the models that display little change in their domain-mean accumulated rain with resolution also do not exhibit much difference in the rain accumulation histograms for the different resolutions. That is not the case for the models that exhibit a peak in the rain accumulation at an intermediate resolution. These exhibit an increased frequency of greater rainrates at these intermediate resolutions (not shown).

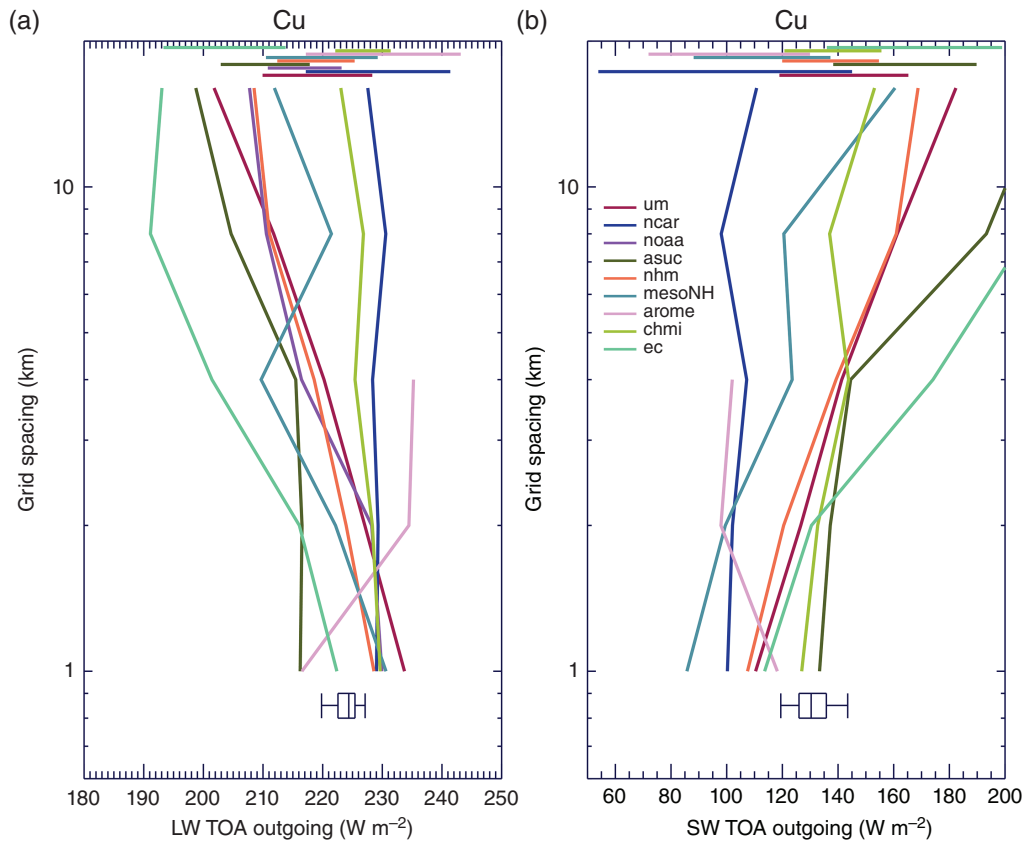


Figure 10. As Figure 5, but for the convective region.

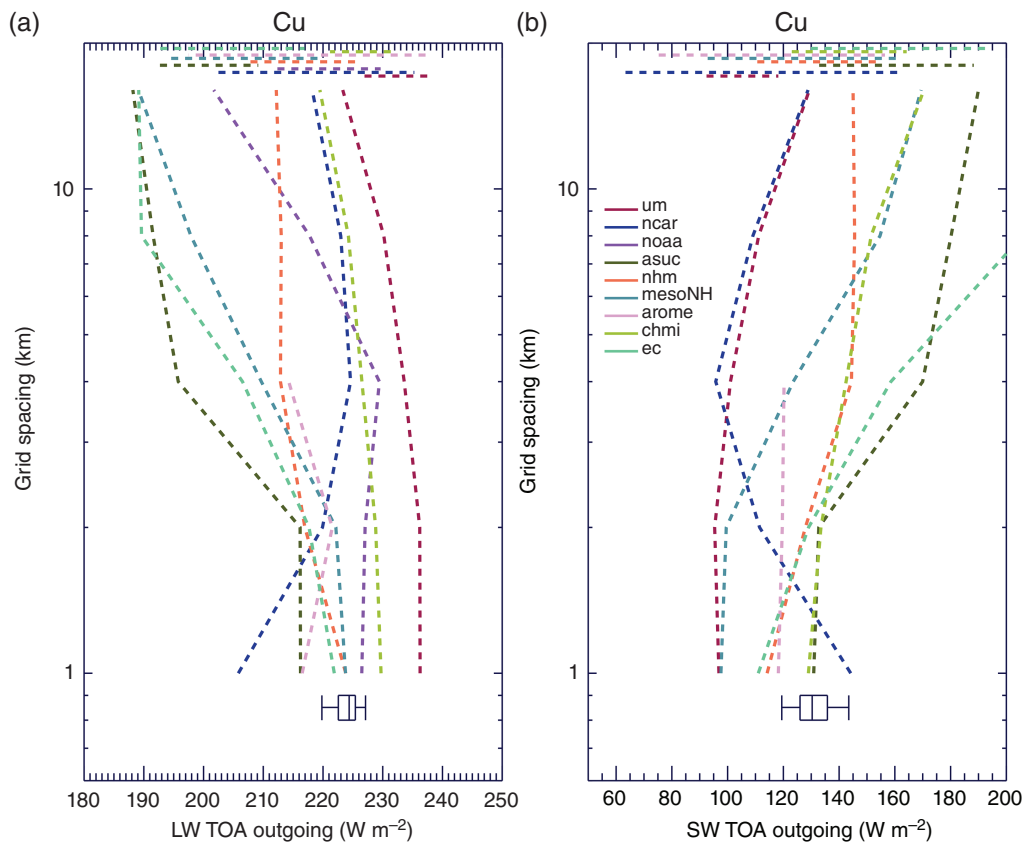


Figure 11. As Figure 6, but for the convective region.

5. Discussion

Comparing first the pairs of models that have the same physics but different dynamical core, it can be seen by looking at the 1 km convection-off long-wave panels in Figures 2–4 that differences in the dynamical core can lead to large differences in the cloud

morphology. Figures 3(e) and (i) show well-developed cloud streets in one simulation (NHM) while the other (ASUCA) has more homogeneous cloud in the stratocumulus region. For the stratocumulus region, this more homogenous cloud for ASUCA translated into improved LWP and radiation comparisons with observations at 1 km model grid spacing. For the cumulus region,

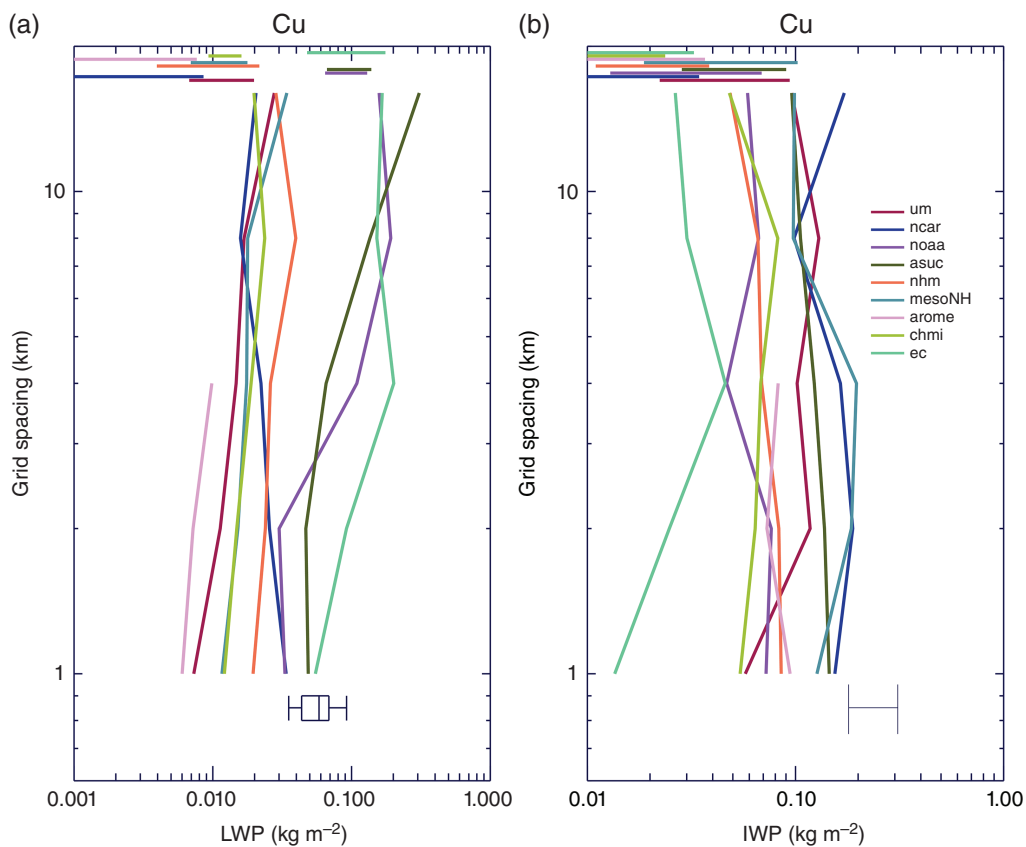


Figure 12. As Figure 7, but for the convective region.

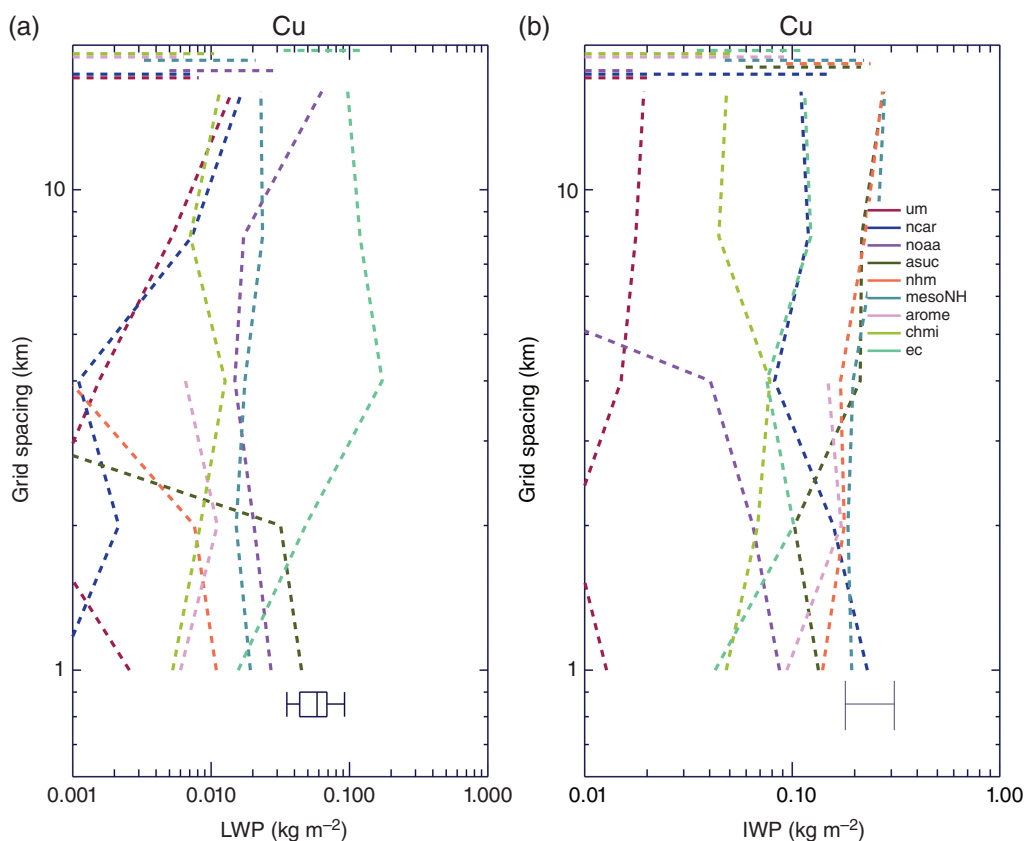


Figure 13. As Figure 8, but for the convective region.

both models have isolated cumulus clouds but ASUCA has improved LWP, IWP and short-wave radiation when compared to observations. In both the cumulus and stratocumulus region, the NHM model has a slightly deeper boundary layer than the ASUCA model.

For the AROME–Meso-NH pair at 1 km, one of the models (Meso-NH, Figure 4(e)) has small but densely spaced cumulus

clouds in the stratocumulus region. The other (AROME, Figure 4(i)) has more layer cloud but it is quite broken and eventually begins to form into wave clouds before breaking up into cumulus further downstream. The Meso-NH model produces better agreement with observations for condensed water, but not for area-averaged radiation. In the cumulus region, the AROME convective elements appears larger than

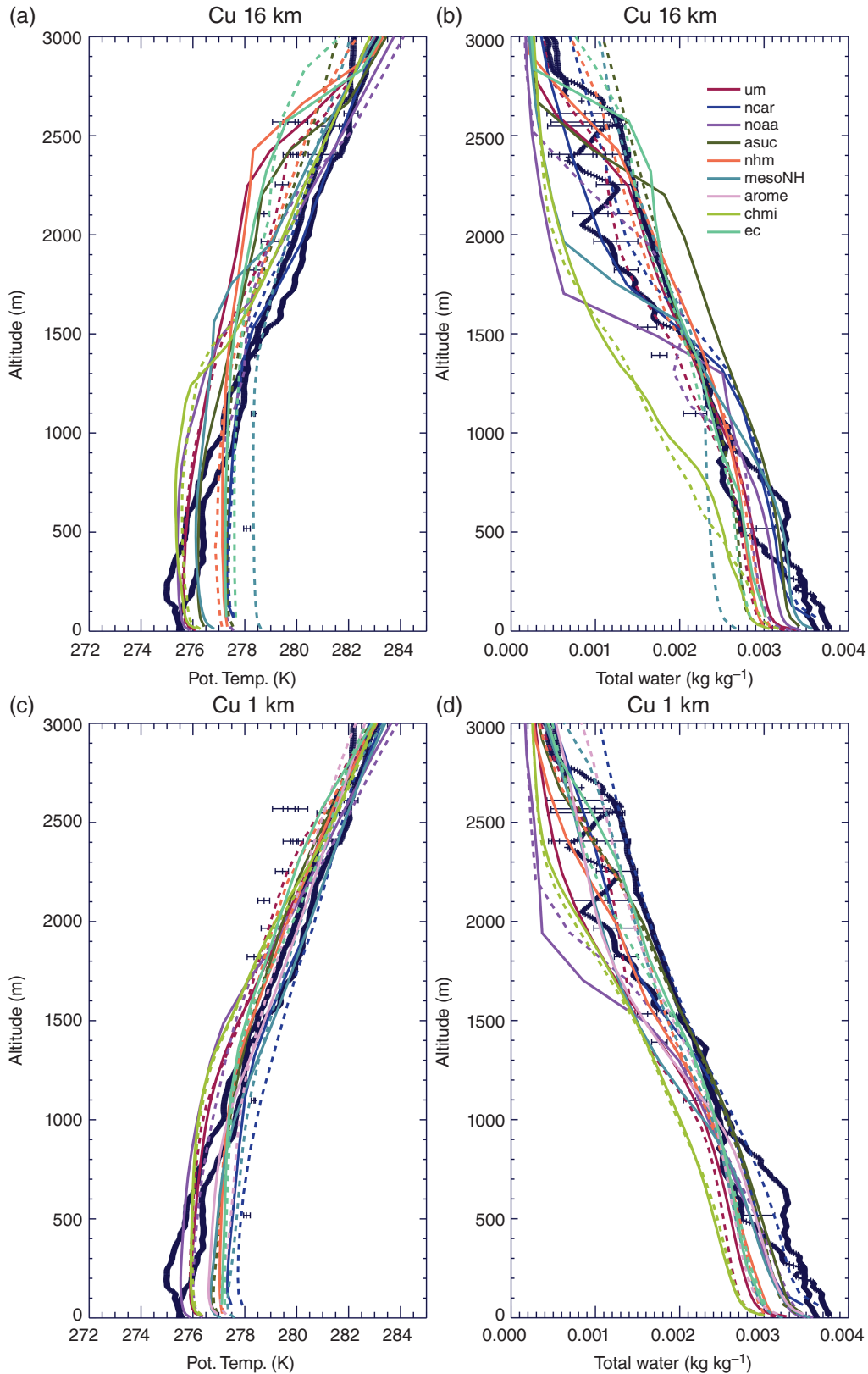


Figure 14. As Figure 9, but for the convective region. The solid circles with error bars are from aircraft measurements and the solid black lines are data from dropsondes (Field *et al.*, 2014).

the Meso-NH convective elements, but the Meso-NH has greater condensed water paths. Both underestimate the LWP, but more accurately reproduce the IWP. These small differences are likely related to the different dynamical formulation adopted in these models and/or the different sources used for initialization and boundary condition of the models (ARPEGE and ECMWF). The main difference between the models at 1 km is that the shallow convection scheme ‘switches off’ at 1 km grid spacing for AROME, leading to identical convection-on/off results, while differences are significant between convection-on and convection-off for

Meso-NH, with better agreement with observations for convection-on (shallow convection only activated).

We turn now to the pair of models with the same dynamical core but different physics. NOAA (Figure 2(e)) and NCAR (Figure 2(i)) both exhibit convective elements in the stratocumulus and convective region. The NCAR convection appears to increase in size more rapidly than the NOAA convective elements. NOAA LWP and long-wave are improved in the stratocumulus region, but the LWP and long-wave are similar in the convective region with the NCAR model exhibiting improved IWP compared

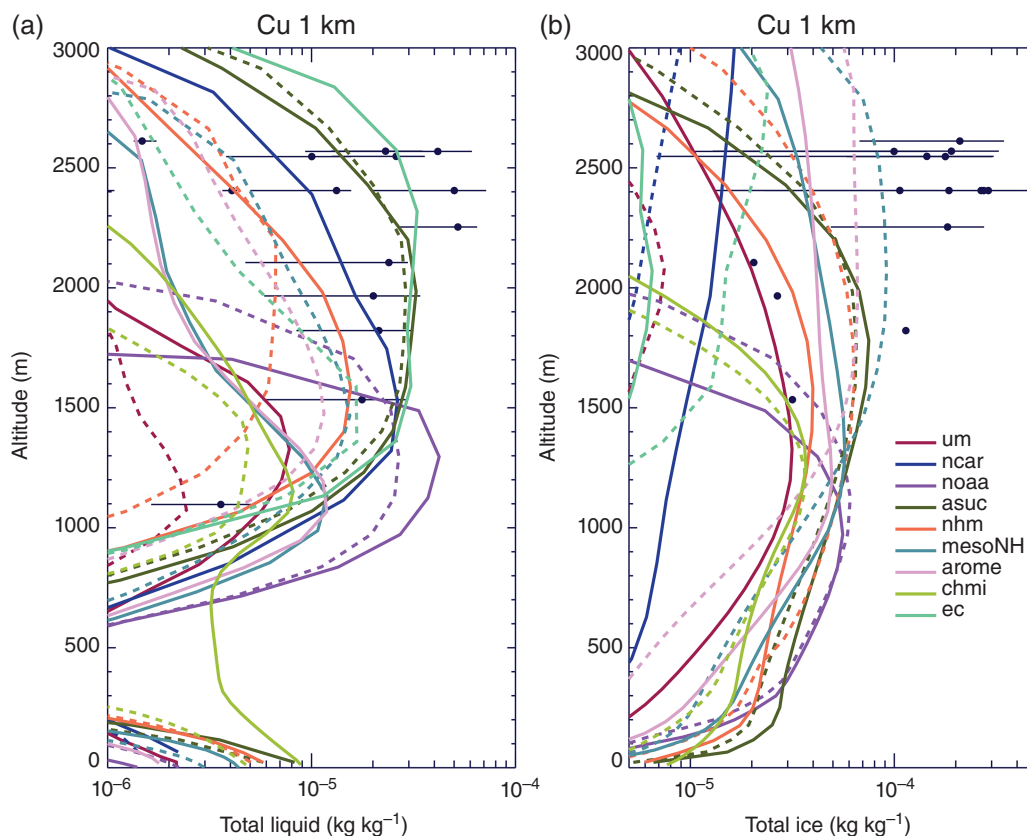


Figure 15. Mean profiles for the convective region for 1 km resolution simulations: (a) total liquid, and (b) total ice. Solid circles represent aircraft observations and the horizontal lines represent the interquartile range for each aircraft leg.

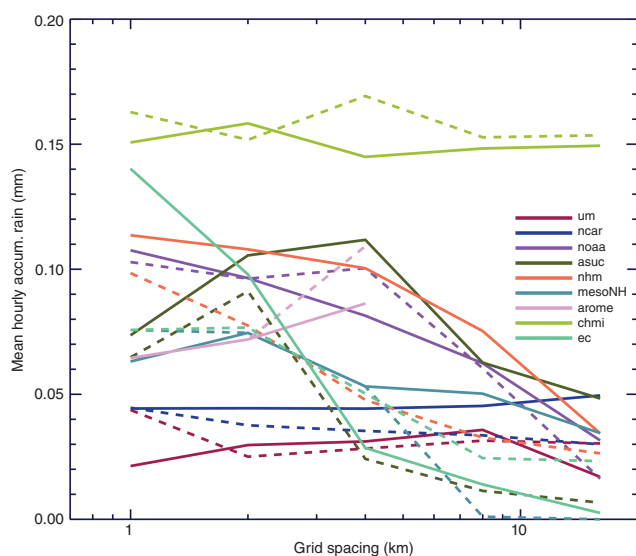


Figure 16. Mean hourly accumulated rain as a function of resolution from three 10 min accumulations at 1050–1100, 1150–1200, 1250–1300 UTC for the region in the convective part of the domain depicted in Figure 1. Solid lines: convection-off simulations, dashed lines: convection-on simulations.

to observations. Sensitivity to the activation of the convection scheme is dramatically different between these two models, with the NCAR model developing more widespread cloud.

In terms of rainrates at 1 km grid spacing in the larger convective region used for Figure 16, it is difficult to conclude whether the pair of models with different physics but the same dynamical core has a larger difference than the pairs of models with the same physics but different dynamical cores. Thus it appears for this case, at 1 km grid spacing and convection-off, that the dynamical core, microphysics and turbulence can play an important role in controlling the morphology of clouds.

Decreases in model spread in terms of the thermodynamic profile and broadband fluxes with decreasing grid spacing as

indicated in Figures 9, 10 and 13 suggest that, for the convection-off simulations, the improved representation of the dynamics is having a positive effect on the quality of the simulations. However, for many metrics, e.g. LWP and IWP, no convergence between the models is seen with resolution.

For the models in this study, the differences in rain accumulation with resolution are quite large and in general have not converged, even at 1 km grid spacing. Moreover, changes in resolution appear to make more difference than variations in model physics when the dynamical core is the same (e.g. NCAR, NOAA) or changes in the dynamics when the physical parametrizations are the same (NHM, ASUCA). Therefore it seems sensible to attempt to understand how the interplay between physics and dynamics, the scale of the phenomenon and the resolution of the model combine to control predictions such as accumulated rain.

The effective resolution is the actual finest well-resolved scale of a model. For a given grid spacing, a model will produce resolved structures depending not only on the grid spacing but also on the diffusion (implicit and explicit) of the model. The difference between the models may come from the numerical schemes (implicit diffusion), but also from the subgrid-transport schemes (explicit diffusion). For instance, due to its efficient but diffusive numerical schemes, AROME's effective resolution is larger than that of Meso-NH (Ricard *et al.*, 2013). Subgrid-transport schemes are the turbulence and convection parametrizations which both limit the variability of the resolved fields. The vertical velocity field is a resolved-field representative of the effective resolution of a model. For instance, it is clear in Figures 2–4 that UM or NCAR present finer structures with convection-off and coarser structures with convection-on, as their convection scheme probably produces strong subgrid updraughts. Vertical velocity is also representative of the partition resolved/subgrid motions. The standard deviation of the vertical velocity field is larger at finer resolutions since more of the flow is explicitly resolved, but for this comparison across scales we have regridded onto a common 16 km grid scale.

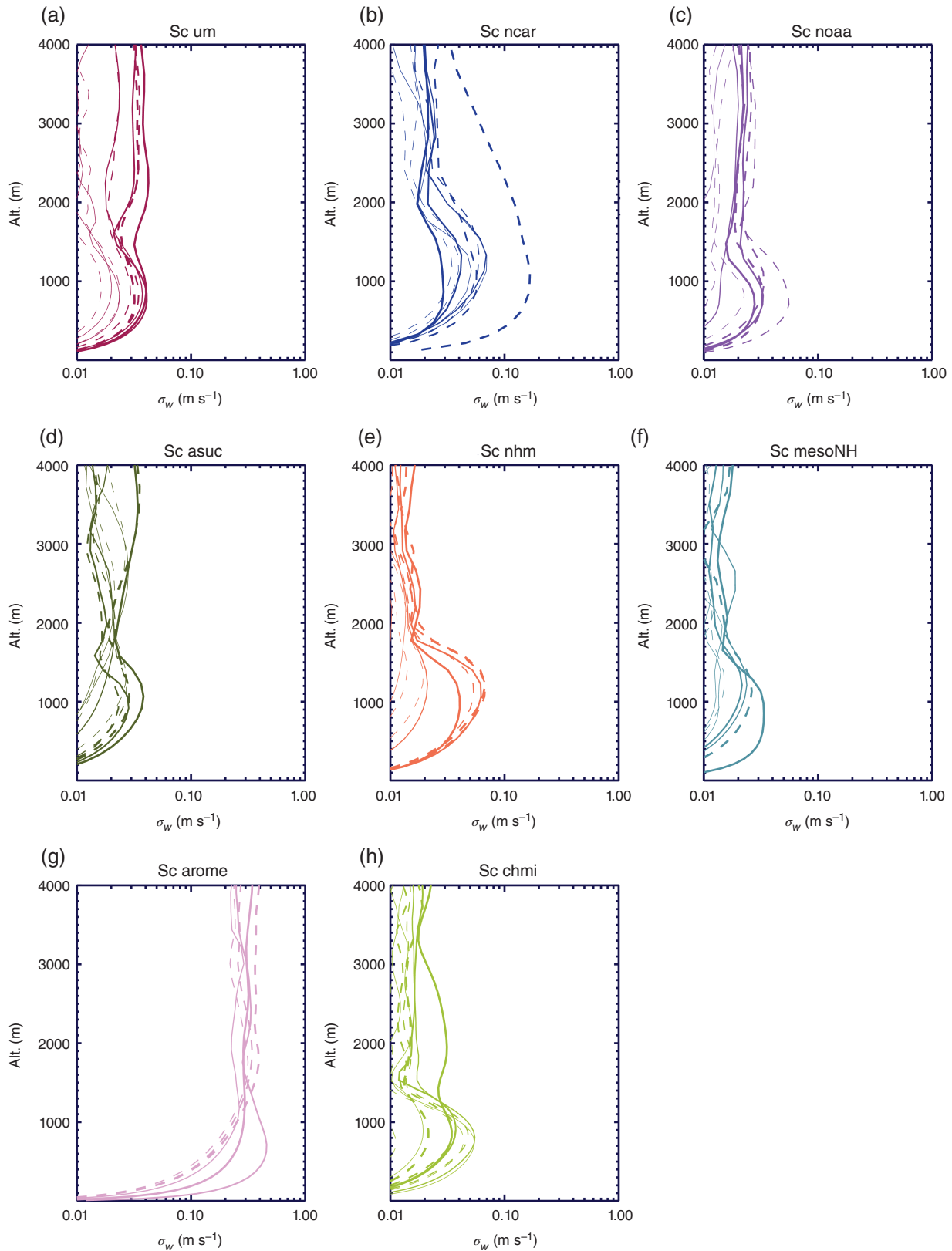


Figure 17. Standard deviation of resolved vertical velocity (σ_w , m s^{-1}) for the stratocumulus region at 1 km for convection-off (solid) and convection-on (dash) simulations for (a) UM, (b) WRF-NCAR, (c) WRF-NOAA, (d) ASUCA, (e) NHM, (f) Meso-NH, (g) AROME and (h) Aladin. The thinnest line is the lowest resolution, and the thickest line is the highest resolution.

The standard deviation of the resolved vertical velocity that has been area-averaged and regridded onto the 16 km resolution grid as a function of altitude and resolution is shown in Figures 17 and 18. It is clear that the standard deviation of the vertical velocity is generally higher in the convective region than in the stratocumulus region, as might be expected. There is a tendency for the vertical velocity standard deviation to be less when the convection parametrization is on than when it is off. Again this might be expected due to the convection parametrization

removing instability from the atmosphere. For the convective region and the convection-on simulations, the UM, NHM, Meso-NH and ALADIN show that the standard deviation increases with increasing resolution, while NCAR, NOAA and ASUCA tend to display a non-monotonic behaviour, with the standard deviation of the vertical velocity increasing at intermediate resolutions. AROME presents the largest values of vertical velocity standard deviation. Differences are less clear for the stratocumulus region, where contributions from other dynamical effects such as gravity

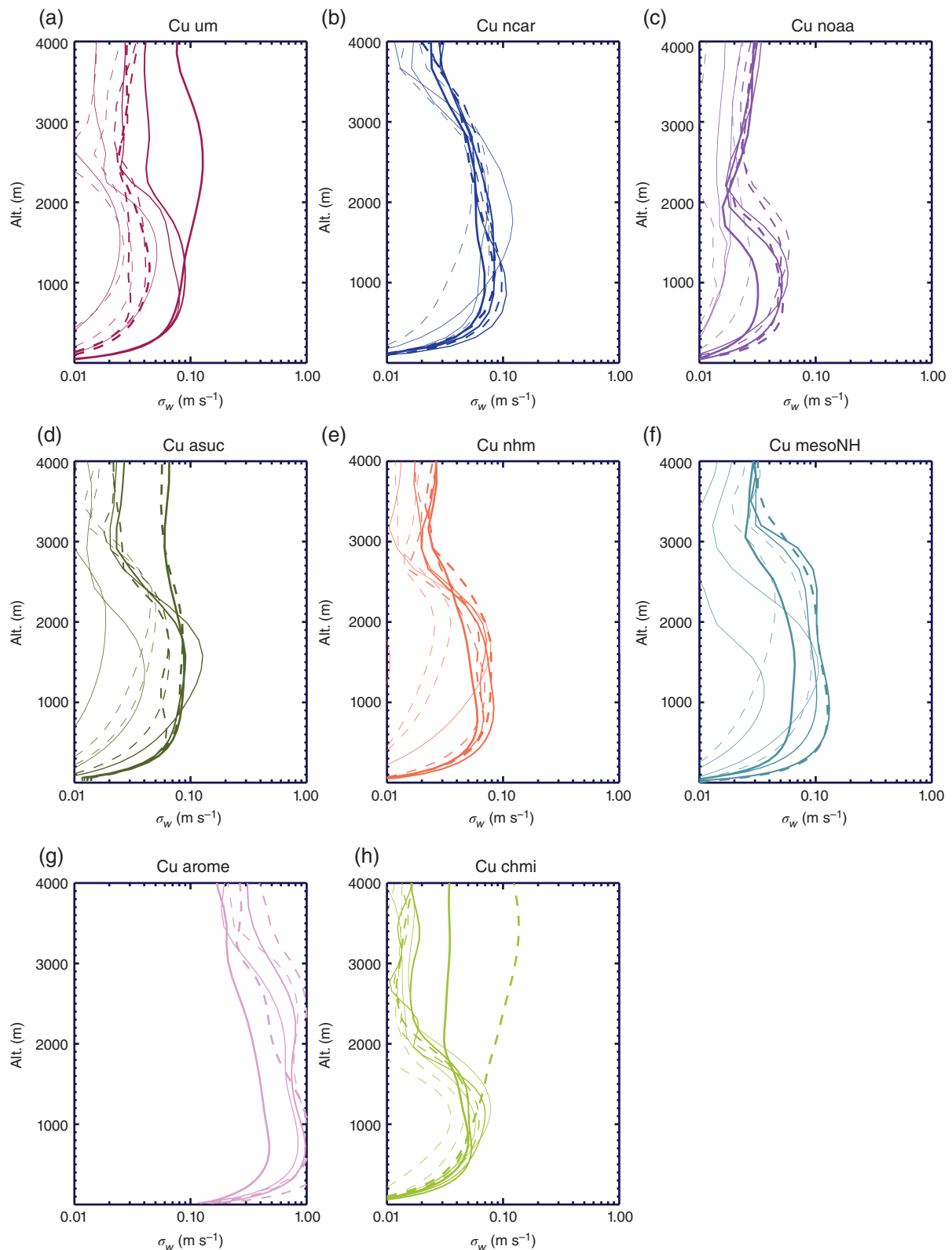


Figure 18. As Figure 17, but for the convective region.

waves and the details of the boundary-layer parametrization will be important.

The simulations mainly fall outside of the grey zone for the stratocumulus region, exhibit a lack of intermodel consistency and poor comparison with the observations. It has been shown in a previous analysis of this case (Field *et al.*, 2014) that forcing the boundary-layer representation to diagnose a well-mixed layer for this region was successful in generating stratiform cloud cover there. In order for the simulations in this region and at these resolutions to capture the behaviour of the cloud and boundary-layer structure in this regime requires an improved boundary-layer parametrization. In contrast, it can be argued

that for the convective region the models are beginning to probe the grey zone in the highest-resolution simulations. For these simulations there is evidence that the models begin to compare better with the observations and converge, as evidenced by the reduction in inter-model spread (e.g. Figures 14 and 10) but without necessarily reaching convergence.

6. Conclusions

A model intercomparison of a cold air outbreak case-study has been performed. The models used included several operational

NWP systems. Simulations were carried out at a range of grid spacings from 16 to 1 km with convection parametrizations on or off and compared to observations at 24 h into the simulation. All of the models and resolutions capture the large-scale structure of the event with a strong northerly cold outflow and a consistent size and location for the polar low feature.

There was more consistency between models for convection-off simulations than for convection-on simulations. This is partly attributed to the differing character of the convective parametrizations: some are scale-aware while others use constant settings appropriate for global model resolutions. However, scale-aware parametrizations can still lead to different precipitation versus model resolution behaviour.

All models struggled to represent the stratocumulus region of the cold air outbreak. There was a lack of model consistency and models tended towards carrying out explicit convection at the highest resolution. This resulted in a tendency for models to generate open cellular structures, a lack of cloud cover and reduced condensed water amounts compared to the observations.

In the convective region, the cloud morphology in all simulations tended towards open cellular convection. For this region, the models showed some convergence for the convection-off simulations and reasonable agreement with the observations in terms of broadband fluxes. For the condensed LWP, the model estimates spanned an order of magnitude but individual models varied much less than this as a function of grid spacing. In addition to generally suffering from a low bias in total condensate mass, only a few of the models were capable of generating sufficient cloud ice at the top of the boundary layer to match the observations.

Comparing pairs of models that share the same physics or dynamical core indicates that both of these model components have strong influences on the morphology, the microphysical and radiative characteristics of the clouds.

The simulations do not really probe the grey zone for the stratocumulus region. Finer grid spacings (~100 m) are required. For km-scale models, a realistic representation of these clouds most likely requires a parametrized approach, such as in the treatment of the boundary layer, to compensate for the models inability to resolve the motions at km-scale and to nudge the models to a more well-mixed boundary-layer solution more appropriate for these stratocumulus clouds. There is greater inter-model agreement and improved comparison with observations for the convective region for some metrics such as broadband fluxes and the thermodynamic structure of the boundary layer. This may be because the grey zone is being probed more successfully by the higher-resolution simulations.

References

- Aranami K, Davies T, Wood N. 2015. A mass restoration scheme for limited-area models with semi-Lagrangian advection. *Q. J. R. Meteorol. Soc.* **141**: 1795–1803.
- Bechtold P, Bazile E, Guichard F, Mascart P, Richard E. 2001. A mass flux convection scheme for regional and global models. *Q. J. R. Meteorol. Soc.* **127**: 869–886.
- Bélaïr S, Mailhot J, Strapp JW, MacPherson IJ. 1999. An examination of local versus nonlocal aspects of a TKE-based boundary layer scheme in clear convective conditions. *J. Appl. Meteorol.* **38**: 1499–1518.
- Bélaïr S, Mailhot J, Girard C, Vaillancourt P. 2005. Boundary layer and shallow cumulus clouds in a medium-range forecast of a large-scale weather system. *Mon. Weather Rev.* **133**: 1938–1960.
- Bénaud P, Vivoda J, Mašek J, Smolíkó P, Yessad K, Smith C, Brožková R, Geleyn J-F. 2010. Dynamical kernel of the Aladin-NH spectral limited-area model: Revised formulation and sensitivity experiments. *Q. J. R. Meteorol. Soc.* **136**: 155–169.
- Benjamin SG, Weygandt SS, Brown JM, Hu M, Alexander CR, Smirnova TG, Olson JB, James EP, Dowell DC, Grell GA, Lin H, Peckham SE, Smith TL, Moninger WR, Kenyon JS, Manakin GS. 2016. A North American hourly assimilation and model forecast cycle: The rapid refresh. *Mon. Weather Rev.* **144**: 1669–1694. <http://dx.doi.org/10.1175/MWR-D-15-0242.1>.
- Bodas-Salcedo A, Williams KD, Ringer MA, Beau I, Cole JNS, Dufresne J-L, Koshiro T, Stevens B, Wang Z, Yokohata T. 2014. Origins of the solar radiation biases over the Southern Ocean in CFMIP2 models. *J. Clim.* **27**: 41–56. <https://doi.org/10.1175/JCLI-D-13-00169.1>.
- Bougeault P, Lacarrère P. 1989. Parameterization of orography-induced turbulence in a mesobeta-scale model. *Mon. Weather Rev.* **117**: 1872–1890.
- Brousseau P, Seity Y, Ricard D, Léger J. 2016. Improvement of the forecast of convective activity from the AROME-France system. *Q. J. R. Meteorol. Soc.* **142**: 2231–2243. <https://doi.org/10.1002/qj.2822>.
- Bryan GH, Wyngaard JC, surFritsch JM. 2003. Resolution requirements for the simulation of deep moist convection. *Mon. Weather Rev.* **131**: 2394–2416.
- Clark PA, Roberts NM, Lean HW, Ballard SP, Charlton-Perez C. 2016. Convection-permitting models: A step change in rainfall forecasting. *Meteorol. Appl.* **23**: 165–181.
- Colella P, Woodward PR. 1984. The piecewise parabolic method (PPM) for gas dynamical simulations. *J. Comput. Phys.* **54**: 174–201.
- Cuxart J, Bougeault P, Redelsperger J-L. 2000. A turbulence scheme allowing for mesoscale and large-eddy simulations. *Q. J. R. Meteorol. Soc.* **126**: 1–30.
- Field PR, Cotton RJ, McBeath K, surLock AP, Webster S, Allan RP. 2014. Improving a convection-permitting model simulation of a cold air outbreak. *Q. J. R. Meteorol. Soc.* **140**: 124–138.
- Gao Y, Leung LR, Zhao C, Hagos S. 2017. Sensitivity of US summer precipitation to model resolution and convective parameterizations across gray zone resolutions. *J. Geophys. Res. Atmos.* **122**: 2714–2733. <https://doi.org/10.1002/2016JD025896>.
- Geleyn J-F, Vana F, Cedilnik J, Tudor M, Cattray B. 2006. An intermediate solution between diagnostic exchange coefficients and prognostic TKE methods for vertical turbulent transport. In *WGNE Blue Book*. WMO: Geneva, Switzerland. <http://www.wcrp-climate.org/WGNE/blue-book.html> (accessed 12 July 2017).
- Geleyn J-F, Cattray B, Bouteloup Y, Brožková R. 2008. A statistical approach for sedimentation inside a micro-physical precipitation scheme. *Tellus A* **60**: 649–662.
- Girard L, Piriou J-M, Brožková R, Geleyn J-F, Banciu D. 2009. Cloud and precipitation parameterization in a meso-gamma-scale operational weather prediction model. *Mon. Weather Rev.* **137**: 3960–3977.
- Girard C, Plante A, Desgagné M, McTaggart-Cowan R, Côté J, Charron M, Gravel S, Lee V, Patoine A, Qaddouri A, Roch M, Spacie L, Tanguay M, Vaillancourt PA, Zadra A. 2014. Staggered vertical discretization of the Canadian Environmental Multiscale (GEM) model using a coordinate of the log-hydrostatic-pressure type. *Mon. Weather Rev.* **142**: 1183–1196.
- Hara T, Kawano K, Aranami K, Kitamura Y, Sakamoto M, Kusabiraki H, Muroi C, Ishida J. 2012. Development of the physics library and its application to ASUCA. *CAS/JSC WGNE Res. Activ. Atmos. Oceanic Modell.* **42**: 5.05–5.07.
- Holloway CE, Woolnough SJ, Lister GMS. 2012. Precipitation distributions for explicit versus parametrized convection in a large-domain high-resolution tropical case-study. *Q. J. R. Meteorol. Soc.* **138**: 1692–1708.
- Hwang Y-T, Frierson DMW. 2013. Link between the double-intertropical convergence zone problem and cloud biases over the Southern Ocean. *Proc. Natl. Acad. Sci. USA* **110**: 13. <https://doi.org/10.1073/pnas.1213302110>.
- Ishida J, Muroi C, Aikawa Y. 2009. Development of a new dynamical core for the nonhydrostatic model. *CAS/JSC WGNE Res. Activ. Atmos. Oceanic Modell.* **39**: 509–510.
- Ishida J, Muroi C, Kawano K, Kitamura Y. 2010. Development of a new nonhydrostatic model ASUCA at JMA. *CAS/JSC WGNE Res. Activ. Atmos. Oceanic Modell.* **40**: 511–512.
- Kain JS, Fritsch JM. 1990. A one-dimensional entraining/detraining plume model and its application in convective parameterization. *J. Atmos. Sci.* **47**: 2784–2802.
- Kolstad EW, Bracegirdle TJ, Seierstad IA. 2009. Marine cold-air outbreaks in the North Atlantic: Temporal distribution and associations with large-scale atmospheric circulation. *Clim. Dyn.* **33**: 187–197.
- Lafore J, Stein J, Asencio N, Bougeault P, Ducrocq V, Duron J, Fischer C, Hérelil P, Mascart P, Masson V, Pinty J-P, Redelsperger JL, Richard E, Vilà-Guerau de Arellano J. 1998. The Méso-NH atmospheric simulation system. Part I: Adiabatic formulation and control simulation. *Ann. Geophys.* **16**: 90–109.
- Lin Y, Farley RD, Orville HD. 1983. Bulk parameterization of the snow field in a cloud model. *J. Appl. Meteorol.* **22**: 1065–1092.
- Lock AP, Brown AR, Bush MR, Martin GM, Smith RNB. 2000. A new boundary-layer mixing scheme. Part I: Scheme description and single-column model tests. *Mon. Weather Rev.* **128**: 3187–3199.
- Mailhot J, Bélaïr S, Charron M, Doyle C, Joe P, Abrahamowicz M, Bernier NB, Denis B, Erfani A, Frenette R, Giguère A, Isaac GA, McLennan N, McTaggart-Cowan R, Milbrandt J, Tong L. 2010. Environment Canada's experimental numerical weather prediction systems for the Vancouver 2010 Winter Olympic and Paralympic games. *Bull. Am. Meteorol. Soc.* **91**: 1073–1085.
- Milbrandt JA, Yau MK. 2005a. A multimoment bulk microphysics parameterization. Part I: Analysis of the role of the spectral shape parameter. *J. Atmos. Sci.* **62**: 3051–3064.
- Milbrandt JA, Yau MK. 2005b. A multimoment bulk microphysics parameterization. Part II: A proposed three-moment closure and scheme description. *J. Atmos. Sci.* **62**: 3065–3081.
- Moore GWK. 2013. A climatology of vessel icing for the subpolar North Atlantic Ocean. *Int. J. Climatol.* **33**: 2495–2507. <https://doi.org/10.1002/joc.3604>.

- Nakanishi M, Niino H. 2009. Development of an improved turbulence closure model for the atmospheric boundary layer. *J. Meteorol. Soc. Jpn.* **87**: 895–912.
- Pearson KJ, Lister GMS, Birch CE, Allan RP, Hogan RJ, Woolnough SJ. 2014. Modelling the diurnal cycle of tropical convection across the 'grey zone'. *Q. J. R. Meteorol. Soc.* **140**: 491–499.
- Pergaud J, Masson V, Malardel S, Couvreur F. 2009. A parameterization of dry thermals and shallow cumuli for mesoscale numerical weather prediction. *Boundary-Layer Meteorol.* **132**: 83–106.
- Pinty J-P, Jabouille P. 1998. 'A mixed-phase cloud parameterization for use in mesoscale non hydrostatic model: Simulations of a squall line and of orographic precipitation'. In Proceedings of Conference on Cloud Physics, 17–21 August 1998 Everett, WA. 217–220.
- Ricard D, Lac C, Riette S, Legrand R, Mary A. 2013. Kinetic energy spectra characteristics of two convection-permitting limited-area models AROME and Meso-NH. *Q. J. R. Meteorol. Soc.* **139**: 1327–1341.
- Saito K, Fujita T, Yamada Y, Ishida J, Kumagai Y, Aranami K, Ohmori S, Nagasawa R, Kumagai S, Muroi C, Kato T, Eito H, Yamazaki Y. 2006. The operational JMA non-hydrostatic mesoscale model. *Mon. Weather Rev.* **134**: 1266–1298.
- Saito K, Ishida J, Aranami K, Hara T, Segawa T, Narita M, Honda Y. 2007. Non-hydrostatic atmospheric models and operational development at JMA. *J. Meteorol. Soc. Jpn.* **85B**: 271–304.
- Sakradzija M, Seifert A, Dipankar A. 2016. A stochastic scale-aware parameterization of shallow cumulus convection across the convective gray zone. *J. Adv. Model. Earth Syst.* **8**: 786–812. <https://doi.org/10.1002/2016MS000634>.
- Seity Y, Brousseau P, Malardel S, Hello G, Bénard P, Bouttier F, Lac C, Masson V. 2011. The AROME-France convective-scale operational model. *Mon. Weather Rev.* **139**: 976–991. <http://dx.doi.org/10.1175/2010MWR3425.1>.
- Skamarock WC, Klemp JB, Dudhia J, Gill DO, Barker DM, Duda MG, Huang X-Y, Wang W, Powers JG. 2008. 'A description of the advanced research WRF version 3', Technical Note 475+STR. NCAR: Boulder, CO.
- Smith RNB. 1990. A scheme for predicting layer clouds and their water content in a general-circulation model. *Q. J. R. Meteorol. Soc.* **116**: 435–460.
- Stein THM, Parker DJ, Hogan RJ, Birch CE, Holloway CE, Lister GMS, Marsham JH, Woolnough SJ. 2015. The representation of the West African monsoon vertical cloud structure in the Met Office Unified Model: An evaluation with CloudSat. *Q. J. R. Meteorol. Soc.* **141**: 3312–3324.
- Termonia P, Fischer C, Bazile E, Bouysse F, Brožková R, Bénard P, Bochenek B, Degrauwe D, Derkova M, El Khatib R, Hamdi R, Mašek J, Pottier P, Pristov N, Seity Y, Smolík P, Spaniel O, Tudor M, Wang Y, Wittmann C, Joly A. 2017. The ALADIN system and its canonical model configurations AROME and ALARO CY40T1. *Geosci. Model Dev.* <https://doi.org/10.5194/gmd-2017-103>.
- Thompson G, Field PR, Rasmussen RM, Hall WD. 2008. Explicit forecasts of winter precipitation using an improved bulk microphysics scheme. Part II: Implementation of a new snow parameterization. *Mon. Weather Rev.* **136**: 5095–5115.
- Tomassini L, Field PR, Honnert R, Malardel S, McTaggart-Cowan R, Saitou K, Noda AT, Seifert A. 2017. The grey zone cold air outbreak global model intercomparison: A cross evaluation using large-eddy simulations. *J. Adv. Model. Earth Syst.* **9**. <https://doi.org/10.1002/2016MS000822>.
- Vaña F, Bénard P, Geleyn J-F, Simon A, Seity Y. 2008. Semi-Lagrangian advection scheme with controlled damping: An alternative to nonlinear horizontal diffusion in a numerical weather prediction model. *Q. J. R. Meteorol. Soc.* **134**: 523–537.
- Walters D, Boutle I, Brooks M, Melvin T, Stratton R, Vosper S, Wells H, Williams K, Wood N, Allen T, Bushell A, Copley D, Earnshaw P, Edwards J, Gross M, Hardiman S, Harris C, Heming J, Klingaman N, Levine R, Manners J, Martin G, Milton S, Mittermaier M, Morcrette C, Riddick T, Roberts M, Sanchez C, Selwood P, Stirling A, Smith C, Suri D, Tennant W, Vidale PL, Wilkinson J, Willett M, Woolnough S, Xavier P. 2017. The Met Office unified model global atmosphere 6.0/6.1 and JULES global land 6.0/6.1 configurations. *Geosci. Model Dev.* **10**: 1487–1520.
- Wentz FJ, Spencer RW. 1998. SSM/I rain retrievals within a unified all-weather ocean algorithm. *J. Atmos. Sci.* **55**: 1613–1627. [https://doi.org/10.1175/1520-0469\(1998\)055<1613:SIRRWAS>2.0.CO;2](https://doi.org/10.1175/1520-0469(1998)055<1613:SIRRWAS>2.0.CO;2).
- Wielicki BA, Barkstrom BR, Harrison EF, Lee RB III, Smith GL, Cooper JE. 1996. Clouds and the Earth's Radiant Energy System (CERES): An Earth observing system experiment. *Bull. Am. Meteorol. Soc.* **77**: 853–868.
- Wilkinson JM, Wells H, Field PR, Agnew P. 2013. Investigation and prediction of helicopter-triggered lightning over the North Sea. *Meteorol. Appl.* **20**: 94–106.
- Wilson DR, Ballard SP. 1999. A microphysically based precipitation scheme for the UK Meteorological Office Unified Model. *Q. J. R. Meteorol. Soc.* **125**: 1607–1636.
- Wood N, Staniforth A, White A, Allen T, Diamantakis M, Gross M, Melvin T, Smith C, Vosper S, Zerroukat M, Thurnburn J. 2014. An inherently mass-conserving semi-implicit semi-Lagrangian discretization of the deep-atmosphere global non-hydrostatic equations. *Q. J. R. Meteorol. Soc.* **140**: 1505–1520.
- Xu KM, Randall DA. 1996. A semiempirical cloudiness parameterization for use in climate models. *J. Atmos. Sci.* **53**: 3084–3102.